Final report submitted to the Texas Water Development Board

Assessing the precursors, persistence and predictability of drought over Texas

By
Dinali Nelun Fernando, Ph.D.

Research undertaken under the aegis of the University Corporation for Atmospheric Research (UCAR) Post-docs Applying Climate Expertise (PACE) Post-doctoral fellowship program

In collaboration with

The Texas Water Development Board
(Water Science and Conservation)

And

The University of Texas at Austin
(Jackson School of Geosciences)

Table of Contents

Acronyms

AMO	Atlantic Multidecadal Oscillation
CAM	Community Atmospheric Model
CCSM	Community Climate System Model
CESM	Community Earth System Model
CFSRR	Climate Forecast System Reforecasts and Reanalysis
CFSv2	Climate Forecast System version 2
CIN	Convective Inhibition
CLM	Community Land Model
CMIP3	Climate Model Intercomparison Project, Phase 3
CMIP5	Coupled Model Intercomparison Project – Phase 5
CPC	Climate Prediction Center
DJF	December, January and February
ENSO	El Niño Southern Oscillation
ERSSTv3b	Extended Reconstructed Sea Surface Temperature version 3b
GFDL	Geophysical Fluid Dynamics Laboratory
GLDAS	Global Land Data Assimilation System
IPSL	Institute Pierre Simon Laplace
JJA	July, July and August
MAM	March, April and May
MERRA	Modern Era Retrospective Reanalysis
MPI	Max Planck Institute
MRI	Meteorological Research Institute
NAO	North Atlantic Oscillation
NARR	North American Regional Reanalysis
NCAR	National Center for Atmospheric Research
NCEP CDAS1	National Centers for Environmental Prediction Climate Data Assimilation System I
NLDAS	North American Land Data Assimilation System
NOAA	National Oceanic and Atmospheric Administration
PCMDI	Program for Climate Model Diagnosis and Intercomparison
PDF	Probability Density Function
PDO	Pacific Decadal Oscillation
POP	Parallel Ocean Program
PRISM	Parameter-elevation Regressions on Independent Slopes Model
RCP	Representative Concentration Pathway
RMSE	Root Mean Square Error
RTM	River Transport Model
SPI6	6 month Standardized Precipitation Index

SST	Sea Surface Temperature
SSTA	Sea Surface Temperature Anomaly
SVD	Singular Value Decomposition
U850	Zonal wind at 850 hPa
V850	Meridional wind at 850 hPa
WCRP	World Climate Research Project
Z500	Geopotential height at 500 hPa

List of figures

List of tables

Scope

This report summarizes the findings of research conducted under the broad theme of "Assessing the precursors, persistence and predictability of drought over Texas" over the period 1 July 2011 to 31 July 2013. At the outset the project had the following goals:

1. Gaining a clearer understanding on the causes of drought in Texas, especially for the drought-of-record that occurred in 1950s;
2. Exploring predictive factors that can be used as an early warning of a drought-of-record scale drought;
3. Reducing uncertainty in projected changes of the hydrological cycle for the state of Texas by identifying models that capture the statistical characterizations and controlling mechanisms of the drought, flood and extreme summer temperature in Texas;
4. Using bias correction and statistical downscaling to reduce uncertainty in projections of future climate inputs, such as surface temperature, rainfall, stream flow and ground water;
5. Determining whether and how statistical characteristics of droughts, extreme temperatures, and floods may change over Texas; and
6. Helping to assess potential impacts to surface water and groundwater resources from climate variability.

Given the intensity of the 2011 drought over Texas, emphasis was placed on goals 1 and 2, with particular focus on understanding the causes of the 2011 drought event and its spring intensification. Research was also undertaken within the framework of goals 3 and 5. Results of the drought predictor research were used to inform the assessment of skill of current generation CMIP5 (Coupled Model Intercomparison Project, Phase 5) models in capturing drought drivers over Texas in the 20th century. The statistical properties of future projected extreme events were assessed using the models that performed better over Texas. Goals 4 and 6 were not addressed during the time period reported.

This report is organized as two parts. Part 1 of this report covers the factors that led to the intense drought event of 2011 and highlights key physical climatic processes that tend to drive droughts of similar magnitude over Texas. Part 2 of the report covers the skill assessment of CMIP5 models in capturing key drought mechanisms in the current day and the likely change in extreme event statistics in the late-21st century.

Executive Summary

Texas experienced its worst one-year drought on record in 2011. Drought was triggered by a La Niña in summer 2010 and a negative North Atlantic Oscillation (NAO) in winter 2010/2011. The NAO drove cyclonic circulation in the eastern US impacting Atlantic sea surface temperatures (SSTs), weakening the low level moisture transport from the Gulf of Mexico into Texas, and reducing winter frontal precipitation. The drought intensified over the spring of 2011 when the La Niña event was transitioning to ENSO-neutral conditions. Extreme drought conditions were established in the summer of 2011 when ENSO-neutral conditions prevailed. Spring drought intensification is attributed to the persistence of ENSO influence on mid-tropospheric stability and surface warmth over southwestern US in the spring. Observational results and experimental runs of the Community Earth System Model (CESM) forced with 2011 sea surface temperature anomalies indicate the establishment of a strong east-west gradient in geopotential height over the southern US that strengthens zonal winds at 850 hPa. These winds advected warmth eastward and resulted in a sharp increase in convective inhibition (CIN) and dewpoint depression over the south central US. The strengthened zonal winds are found in other severe-to-extreme drought events with rainfall deficits extending from winter to spring. The persistence of drought over the summer of 2011 is attributed to SST anomalies in the North Pacific and to the establishment of a mid-tropospheric ridge over the south central US, attributed to large cumulative soil moisture deficits. Observational analysis indicates that soil moisture deficits in May can drive the establishment of a mid-tropospheric ridge approximately one month later over the south central US. The drought diminished in the winter of 2011/2012 despite a consecutive La Niña event, which was established in the fall of 2011 and persisted through February 2012. Drought demise is attributed to a positive NAO that drove anticyclonic circulation in the Atlantic and strengthened low-level moisture transport from the Gulf of Mexico. The complex interplay between Pacific and Atlantic SST anomalies, atmospheric circulation, and land surface feedbacks underscores the difficulty of predicting droughts in this region.

We assessed the skill of nine climate models that participated in the Coupled Model Intercomparison Project-Phase 5 (CMIP5). These models have a realistic representation of the seasonal cycle, probability distributions of surface daily maximum and minimum temperature (Tmax, Tmin), precipitation (P) and evapotranspiration (ET) over the south-central United States (SC US) and the 500 hPa geopotential height (Z500) and 850 hPa winds in winter and fall. However, they have wet and cold biases in P and Tmax, underestimate non-rainy days and heavy rainy days and overestimate moderate rainrate events. Half of these models underestimate weak negative P-ET and strong positive P-ET. Wet and cold biases are consistent with uncertainty in the modeled pattern of Z500 and 850hPa winds in summer. Most models cannot realistically capture the seasonal dependence of rainfall anomalies over the SC US on the El Niño-Southern Oscillation (ENSO), the observed global SST warming mode and its relationship with an increase of summer rainfall over the SC US. The models that cannot adequately capture the processes that control regional climate variability and change also tend to be the outliers in climate projections for the SC US. The models consistently project a disproportionally strong increase in Tmax ranging from 28˚C to 43˚C (82.4˚F to 109.4˚F) and in Tmin ranging from 25˚C- 30˚C (77˚F - 86˚F), an increase of non-rainy days and a decrease of medium rainrate events. The ensemble projections suggest decreases of P-ET during all seasons except for summer. Excluding the under-performing models leads to a stronger drying of P-ET.

Part 1: The evolution of the 2011 Drought over Texas and Implications for Drought Predictability[1]

1.1: Introduction

In 2011, Texas suffered the worst drought in recent decades. Drought conditions lasted for more than a year and covered five states over the southern United States. The economic impact of this drought on Texas is estimated at 7.6 billion dollars (Fannin 2012), primarily caused by crop and livestock losses. The losses were almost twice the previous single-year record of $4.1 billion set in 2006. Rainfall during the period from October 2010 to September 2011 was 40% below normal (286 mm), relative to the period of 1898-2011 (http://www.ncdc.noaa.gov/sotc/drought/2011/8). Such a departure in annual rainfall over a water year (i.e. October-September) resulted in the 2011 drought being classified as the "worst one-year drought on record". Dry conditions were also accompanied by record heat in the summer with a mean June, July, August (JJA) temperature of 30.4 C, exceeding the long term mean by 2.9°C (approximately double the previous record of 1.6°C departure established in 1998) (Hoerling et al., 2013). The dry and hot conditions exposed the vulnerability of the state's electricity generation capacity that is heavily reliant on water for cooling and is isolated from the US national grid (Stillwell et al. 2010). Understanding factors that led to the development of the drought is critical for natural resources management and policy development.

The 2011 drought was unusual because of its rapid intensification over late spring to early summer [Fig. 1.1(f)] and unexpected recovery during winter 2011/2012 [Fig. 1.1 (k and l)] as indicated by the 6-month standardized precipitation index which corresponds well with the US Drought Monitor. In January to March (JFM) of 2011, extreme drought (D3 category) covered about 43% area of the state. It spread rapidly to 73% area of the state during April to June (AMJ), and to 97% by the early October with 88% of the state in exceptional drought (D4 category, < 3% likelihood of occurring, http://droughtmonitor.unl.edu/archive.html). Such rapid intensification of the 2011 drought caused statewide reservoir storage to plummet to 58% in November 2011, the lowest since 1978 [*Texas Water Development Board, 2010; Texas Water Development Board, 2011(a) and (b)*]. The quick depletion of water storage caught water managers by surprise because the state reservoir system was designed to withstand the worst multi-year drought such as the 1950s drought of record. The extreme drought conditions ended unexpectedly with a wet winter (2011/2012) despite a continuation of La Niña conditions until February 2012.

Texas has two rainfall regimes. Eastern Texas is humid with two rainfall peaks in May and September and a mean annual rainfall of 1187mm. West Texas is semi-arid with a rainfall peak in summer and a mean annual rainfall of 355mm. With such a low annual rainfall, West Texas is more susceptible to persistent drought than other parts of the state. Drought in Texas often occurs during

---

[1]Part 1 includes material from 'Fernando, D.N., Mo, K., Fu, R., Scanlon, B.R., Solis, R.S., Yin, L., Ren, T., Zhang, K., Bowerman, A., Mace, R., and Mioduszewski, J.R. *Evolution of the 2011 Drought over Texas and Implications for Predictability Texas Drought'* (To be submitted to Journal of Hydrometeorology).

cold El Niño Southern Oscillation (ENSO[2]) – known as La Niña – events (Ropelewski and Halpert, 1989). Overall, drought onset is more predictable than demise. Over the Southern Plains, a La Niña event usually occurs one season before the onset of drought. In general, there are no drought events during warm ENSO (El Niño) years (*Mo* 2011). The only exception is the 1998 extreme summer drought event that took place on the heels of the 1997/98 El Niño event. This exceptional event has been attributed to internal atmospheric dynamics and soil moisture feedback processes (Hong and Kalnay, 2002). The occurrence of a La Niña can usually serve as an early warning for drought over the southern plains.

Hoerling et al. (2013) analyzed factors, including climate change, that led to the 2011 drought over Texas attaining the magnitude and intensity it did over the summer (June through August, JJA) months. They indicate that the extreme precipitation deficits in the winter/spring and summer, related to anomalous SSTs associated with the La Niña event in the Tropics, set up antecedent and concurrent conditions for the record breaking heat wave in summer 2011. They further state that while SSTs greatly increased the probability for an extremely hot and dry summer, approximately 20% (or 0.6C of the 2.9C anomaly) of the magnitude of the JJA heat wave could be attributed to global climate change. They also indicate that the dry conditions of JJA 2011 are contrary to the historical trend over the south central US, which shows a mean increase in summer precipitation.

---

[2] The Climate Prediction Center of the National Centers for Environmental Prediction provide the following definitions of ENSO, its warm phase (El Niño), its cold phase La Niña and ENSO-neutral: "The ENSO cycle refers to the coherent and sometimes very strong year-to-year variations in sea- surface temperatures, convective rainfall, surface air pressure, and atmospheric circulation that occur across the equatorial Pacific Ocean. El Niño and La Niña represent opposite extremes in the ENSO cycle. El Niño refers to the above-average sea-surface temperatures that periodically develop across the east-central equatorial Pacific. It represents the warm phase of the ENSO cycle, and is sometimes referred to as a Pacific warm episode. La Niña refers to the periodic cooling of sea-surface temperatures across the east-central equatorial Pacific. It represents the cold phase of the ENSO cycle, and is sometimes referred to as a Pacific cold episode. ENSO-neutral refers to those periods when neither El Niño nor La Niña is present. These periods often coincide with the transition between El Niño and La Niña events." For monitoring purposes, warm and cold episodes are based on a threshold of +/- 0.5^{o}C for the Oceanic Niño Index (ONI) [3 month running mean of SST anomalies in the Niño 3.4 region (5°N-5°S, 120°-170°W)].Warm and cold episodes are defined when the threshold is met for a minimum of 5 consecutive over-lapping seasons. The four regions of the Pacific ocean used for monitoring ENSO-related SSTs are available at:
http://www.cpc.ncep.noaa.gov/products/analysis_monitoring/ensostuff/nino_regions.shtml
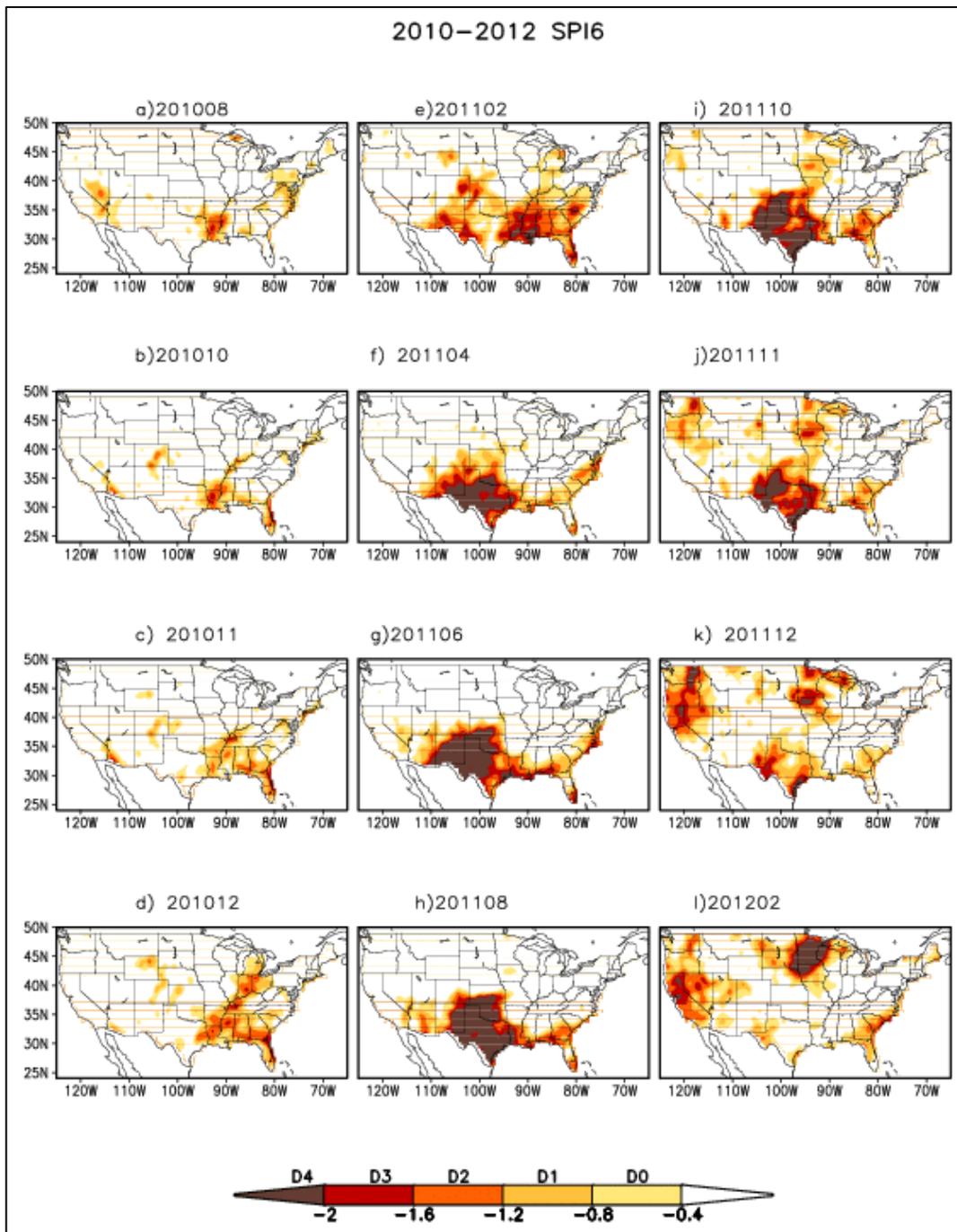
Figure 1.1: 6-month standardized precipitation index (SPI6) for (a) August 2010, (b) October 2010 (c) November 2010, (d) December 2010, (e) February 2011, (f) April 2011, (g) June 2011, (h) August 2011, (i) October 2010, (j) November 2011, (k) December 2011, and (l) February 2012. Drought Monitor D0-D4 categories associated with SPI6 values are provided in the scale bar.

While the La Niña event may have been the trigger of the drought event, the evolution of the drought cannot be attributed entirely to La Niña. For example, the drought intensified over late-spring/early-summer when the La Niña event was waning; and the drought peaked in intensity in the summer months when ENSO was in a neutral state [Fig. 1.2 (a) and (b)]. Seager et al. (2014) demonstrate that precipitation anomalies over Texas and northern Mexico in 2011 exceeded deficits typical during La Niña events. They find that SSTAs in the tropical Pacific cannot explain the observed drought intensification in the summer and pinpoint a probable role for internal atmospheric variability or strong local land-atmosphere coupling in driving such intensification. A La Niña event returned in the fall of 2012 and strengthened in the winter of 2012. However drought conditions diminished unexpectedly in the winter of 2011/2012 despite the ongoing La Niña. Therefore, it is clear that SSTAs associated with La Niña alone do not adequately explain drought evolution.

Studies show that SSTAs in the North Pacific can influence summer rainfall over the United States. For example, Ting and Wang (1997) identified two Singular Value Decomposition (SVD) modes associated with rainfall over the United States. The first is an ENSO mode. The second mode links rainfall in Oklahoma and the Tennessee Valley to SSTAs in the North Pacific. Using the Palmer Drought Severity Index (PDSI) as an indicator for drought, Barlow et al. (2001) studied the relationship between SSTAs and drought in the summer. They found that in addition to ENSO, both the Pacific Decadal Oscillation [PDO[3], Mantua et al., 2002] and North Pacific SSTAs are linked to drought over the Southwest and Texas.

---

[3] The Pacific Decadal Oscillation (PDO) refers to a long-term ENSO-like variability in the Pacific Ocean. It is characterized by a seesaw of SSTs between the North Central Pacific and the Pacific coast of North America. A negative or cool phase of the PDO is characterized by above normal SSTs the north central Pacific and below normal SSTs off the Pacific northwest coast of the US. A positive or warm phase of the PDO is associated with below normal SSTs in the north central Pacific and above normal SSTs off the US Pacific northwest coast (http://jisao.washington.edu/pdo/). A cycle, or a particular phase, typically lasts 20-30 years. At present, a negative phase is in place, which typically results in warmer temperatures and less rainfall over the southern US and northern Mexico.
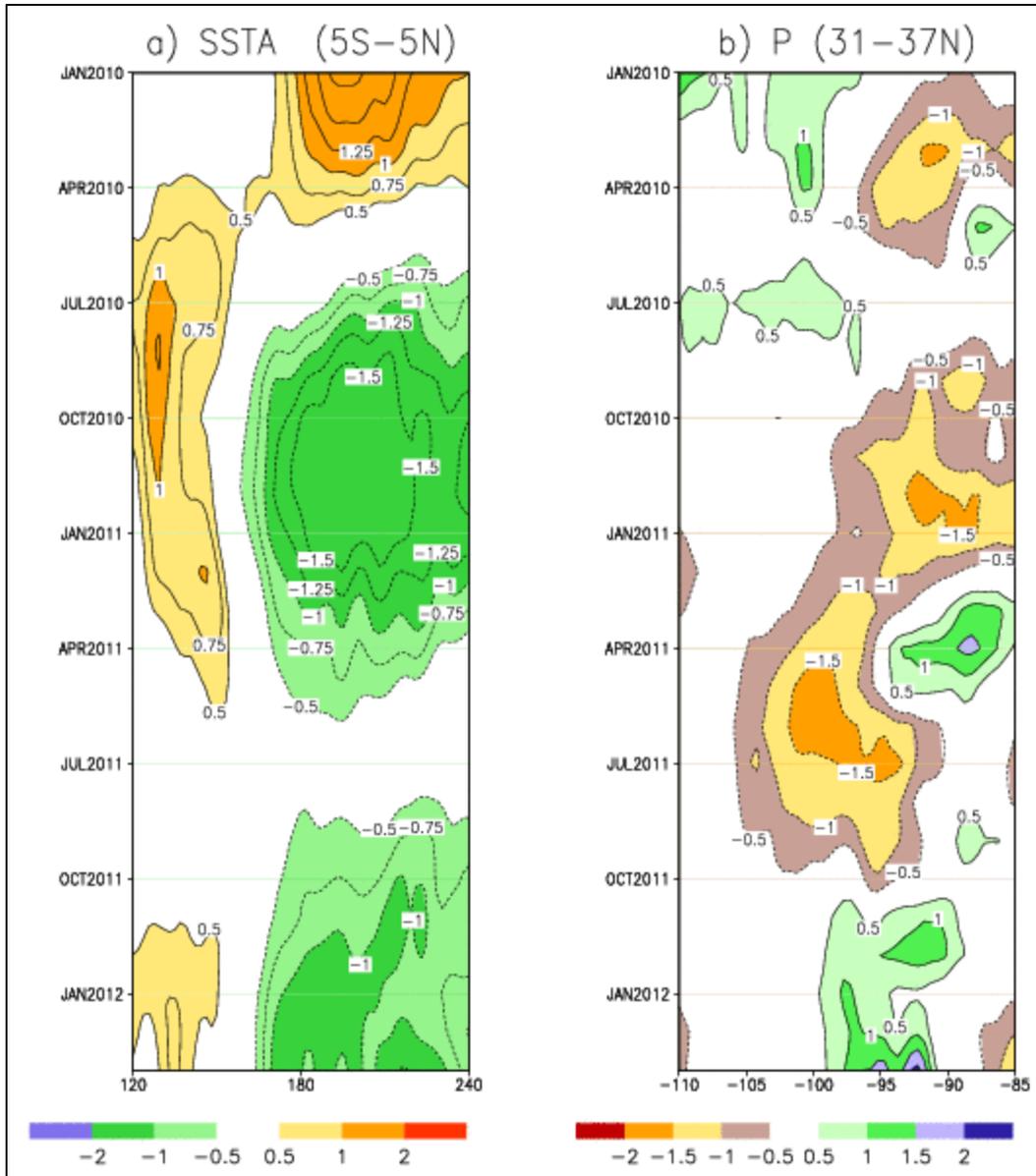
Figure 1.2: (a) Time longitude plot of SSTAs over the longitudes 120W-240W (Pacific Ocean) and averaged over the latitudes 5S to 5N from Jan 2010 to Jan 2012. Contour interval is 0.5° C . Zero contours are omitted, (b) same as (a), but for precipitation anomalies over the longitudes -110W to -85W (central US) and averaged over the latitudes 31N-37N from Jan 2010 to Jan 2012. Contour interval is 0.4 mm day^{-1}. Zero contours are omitted.

In addition to SSTAs in the Pacific, SSTAs in the Atlantic can also influence rainfall in the southern US (Enfield at al.1997). Circulation anomalies associated with the warm phase of the Atlantic Multidecadal Oscillation [AMO[4], Enfield et al., 2001], when warmer than normal SSTs prevail in the tropical north Atlantic, lead to severe dry conditions over the southern plains (Hu and Feng, 2012). Positive SSTAs in the tropical Atlantic will enhance the impact of cold ENSO events on precipitation over the southern United States [*Mo et al.* 2009, *Shubert et al.* 2009]. On the decadal time scales, there is an association between the Atlantic and Pacific SSTAs with the Atlantic SSTAs lagging the Pacific by 6 months (Mo and Hakkinen 2001).

What causes the intensification of drought over the summer? Some studies have suggested regional land-atmosphere feedback as a contributor to drought intensification [*Lyon and Dole, 1995; Hong and Kalnay, 2002*]. Dry soils caused by the cumulative impact of deficit precipitation and net surface heating can, in turn, further enhance precipitation deficits [*Mueller and Seneviratne, 2012*]. Modeling analyses have identified the central US, including much of Texas as an area of strong coupling between soil moisture and precipitation [*Koster et al., 2004*]. Convective precipitation is more sensitive to soil moisture variations than large-scale precipitation [Zhang et al., 2008(b)]. Convective Inhibition (CIN) has been identified as the primary condition that controls summer drought over Texas. It has also been suggested that summer drought is maintained by the modulation of the convective inhibition (CIN)[5] by soil moisture, which in turn leads to less convection and less rainfall [Myoung and Nielsen-Gammon, 2010]. Several other studies have attributed summer drought over the central US to high pressure systems forced either by remote SST-driven anomalous large-scale circulation patterns [*Trenberth et al., 1988*] or by the eddy-mean flow interaction [*Lyon and Dole, 1995; Mo et al., 1991*]. Hoerling et al. (2013) showed a robust linear relationship between the heat waves and drought over Texas, suggestive of feedback mechanisms between temperature and precipitation. While the relationship between temperature and precipitation is clear, the feedback mechanisms are still not fully understood. A heat wave may also increase the stability of the atmosphere because intensified surface heating due to a reduction in soil moisture can, in the absence of cooling in the upper troposphere, influence the establishment of a mid-tropospheric high pressure system (hence, mid-atmospheric stability) as a compensating effect to a thermal low pressure system at the surface [*Oglesby and Erickson III, 1989; Lupo and Bosart, 1999*]. Such mid-atmospheric stability can hamper convective precipitation.

In this paper, we will briefly review the evolution of the 2011 Texas drought and discuss the physical mechanisms associated with the different phases of the drought. The impact of soil moisture anomalies on drought intensification and persistence and the role played by SSTAs in the Atlantic and Pacific in sustaining and relieving drought conditions are also discussed. We specifically investigate the role of SSTAs on 500 hPa geopotential height[6] anomalies, and the influence of soil moisture anomalies on surface temperature anomalies, to deduce factors that could have led to the establishment of the high pressure system at 500 hPa in April 2011 and its persistence through JJA 2011. Factors that led to

---

[4] The Atlantic Multidecadal Oscillation (AMO) refers to long duration changes, typically on the order of 20-40 years, in SSTs in the north Atlantic Ocean. A warm phase of the AMO, as has been in place since 1995, is associated with drought in the south, southwest and Midwest of the US.

[5] Convective Inhibition (CIN) is the energy needed to lift a parcel of air from its level of origin to the level of free convection (source: http://glossary.ametsoc.org/wiki/Convective_inhibition).

[6] Geopotential height approximates the height of an atmospheric pressure surface above mean sea level. Cold air masses are more dense than warm air masses. Therefore, heights are lower in the presence of cold air masses and higher in warm air masses. Geopotential height anomalies are departures from average values of heights for a given pressure surface.

spring intensification are discussed in detail within the context of past drought events that have affected Texas. We place a particular emphasis on identifying large-scale forcing factors and proximate causes that drive the intensification. Our ultimate goal is to improve current understanding of processes driving drought intensification in the spring and summer so that drought predictability at the seasonal timescale could be enhanced. Understanding how the 2011 events fits within a global change perspective is not within the scope of this paper and readers are referred to Hoerling et al., (2013) for a thorough exposition on this subject. The manuscript is organized as follows: section 1.2 describes the datasets and methodology used; section 1.3 discusses the key characteristics of drought onset, intensification and demise, and addresses the key physical processes that appear important at each stage; section 1.4 summarizes the main findings.

1.2: Data and methods

Three precipitation data sets are used for this study. One is the Climate Prediction Center (CPC) unified precipitation data set (*Xie et al*. 2010) from 1950-2010 available at 0.5°x0.5°resolution. The second is the precipitation analysis from the University of Washington based on index stations (Maurer et al. 2002). It covers the period from 1915-2010 and is available at 1/8° resolution (~12 km). The third is the monthly rainfall product from PRISM (http://www.prism.oregonstate.edu/) available at 4 km resolution covering the period 1895-2012. The indicator used to track drought evolution from 2010 to 2012 is the 6-month Standardized Precipitation Index (SPI6) computed from precipitation data sets using the procedure by Mckee et al. (1993; 1995). SPI6 values corresponding to the US Drought Monitor drought classification are: D1(moderate drought) $-0.8 \geq SPI6 \geq -1.2$, D2 (severe drought) $-1.3 \geq SPI6 \geq -1.5$, D3 (extreme drought) $-1.6 \geq SPI6 \geq 1.9$, and D4 (exceptional drought) $-2.0 \geq SPI6$ (http://www.cpc.ncep.noaa.gov/products/Drought/Monitoring/spi.shtml). Precipitation anomalies are calculated using the above mentioned Xie et al. (2010) dataset with a monthly climatology for the 1950 to 2010 base period. We track the evolution of soil moisture and surface temperature anomalies using ensemble means of total soil moisture, evaporation, sensible heat and 2-meter Temperature (T2m) derived from four land models (Noah, Vic, Mosaic and Sac) taken from the National Centers for Environmental Prediction (NCEP) North American Land Data Assimilation System [*NLDAS, Xia et al., 2011*]. Drought onset, with respect to precipitation and soil moisture anomalies, is defined as when normalized precipitation anomalies are less -0.8 and column soil moisture is less than its 20th percentile for a given month. The vertically integrated moisture fluxes were obtained from the North American Regional Reanalysis (NARR) [*Mesinger and co-authors, 2006*]. The NCEP NLDAS and the NARR cover the period from 1979 to the present. Most other atmospheric variables such as geopotential heights and wind fields are from the NCEP-CDAS1 [*Kalnay et al. 1996*] with the base period from 1950-2010. The SST data set is the Extended Reconstructed Sea Surface Temperature (ERSST) version 3b (v3b) and the monthly climatology was computed for the base period from 1915 to 2010 (*Smith et al.* 1996). The Pacific Decadal Oscillation index (Mantua et al. 1997) was downloaded from http://jisao.washington.edu/pdo. We use the Maurer et al. (2002) precipitation analysis to test the correlation between the PDO and SPI6. The Nino3.4 and Nino4 indices were downloaded from http://iridl.ldeo.columbia.edu/SOURCES/.Indices/.nino/.EXTENDED/. The Atlantic Multidecadal Oscillation Index was downloaded from http://www.esrl.noaa.gov/psd/data/correlation/amon.us.long.data.

Droughts of similar magnitude to the 2011 drought are identified by obtaining the standardized anomalies of 12-monthly precipitation from October through September over the period 1895-2011. The monthly PRISM rainfall product at 4 km resolution over the domain 106.8°W to 93.5°W and 25.5°N to 36.8°N was used to calculate the spatial mean monthly precipitation prior to generating the standardized anomalies. The entire period of record (1895-2011) was used as the baseline to calculate the mean and standard deviation. Next the season with the most pronounced rainfall reduction was identified. Seasons are delineated as fall (SON), winter (DJF), spring (MAM), summer (JJA) and the rainy season (April through September). Rainfall in each season in 2011 was compared with seasonal rainfall in other extreme drought years. Percent normal (total seasonal rainfall divided by mean seasonal rainfall for 1895 – 2011) was the metric used for comparison. The contribution of seasonal rainfall anomalies to severe ($-3 \leq PDSI \leq -2$) and extreme ($PDSI \leq -3$) droughts was determined. Past droughts were characterized based on seasonal rainfall anomalies and persistence and/or cessation of the anomaly in adjacent seasons (i.e. MAM_{dry} to JJA_{dry}, MAM_{dry} to JJA_{wet}, etc.). The chi-squared test was used to establish whether there is a significant preference for dry springs to drive the persistence of below normal rainfall from winter through spring. The transition categories subjected to the chi-squared test are $DJF_{dry}|MAM_{dry}|JJA_{dry}$ and $DJF_{dry}|MAM_{wet}|JJA_{dry}$.

The seasonal cycle of convective inhibition (CIN) was studied over Texas at pentad (5-day) timescales during past extreme droughts, non-droughts, and in 2011. Six-hourly CIN fields from the NOAA 20th Century Reanalysis version 2 [*20CRv2, Compo et al., 2011*] were averaged to pentads to cover past droughts and non-droughts from 1895-2008. Pentad CIN fields for 2011 were derived from the monthly real-time forecasts organized as daily starts of four members from the Climate Forecast System version 2 [*CFSv2, Saha et al., 2014*]. CIN is strongly correlated with surface dewpoint temperature [*Myoung and Nielsen-Gammon, 2010*]. The covariability of CIN and lower-tropospheric temperature fields in 2011 were studied using 2-meter dewpoint depression and 850 hPa temperature anomalies. Dewpoint depression was derived using 2-meter temperature and 2-meter dewpoint from CFSv2 monthly real-time fields. 850 hPa temperature anomalies are from NCEP-CDAS1. We use a climatology of 1981-2010 for these fields. CIN and temperature fields were averaged over the spatial domain 25°N-38°N and 108°W-93.5°W.

The low-level (850 hPa) wind vector at pentad timescales was evaluated to assess factors that control dewpoint and air temperature at the surface and resultant CIN. Winds at 850 hPa for select pentads in April through June and at monthly timescales for April through July were evaluated to identify the large-scale circulation anomaly that contributed to the anomalous CIN. The evolution of the 500 hPa geopotential height was tracked in 2011 over Texas using NCEP-CDAS1 daily fields of geopotential height at 500 hPa averaged into pentads. We also use monthly fields of potential temperature from CFSRR and relative vorticity from NCEP-CDAS1 to track the eastward advection of temperature and vorticity anomalies in April 2011.

To ascertain the role that SSTAs in 2011 played on observed circulation anomalies over Texas in April and May, we compare a control run from the National Center for Atmospheric Research (NCAR) Community Earth System Model version 1.1.1. (CESM 1.1.1) versus an experimental run with 2011 SSTA forcing. The CESM is a fully-coupled global climate model that is composed of six geophysical models which simultaneously model the Earth's atmosphere [Community Atmosphere Model (CAM) developed from NCAR CCSM3], ocean [an extension of the Parallel Ocean Program (POP) version 2 from Los Alamos National Laboratory], land [the Community Land Model (CLM) developed by NCAR Climate and Global Dynamics Division and the CESM Land Model Working Group], sea ice [an extension of the sea-ice model at Los Alamos National Laboratory], river-runoff [River Transport Model (RTM)], and land ice [an extension of the Glimmer Ice Sheet Model]. It also includes a coupler component that coordinates the

time evolution of the geophysical models and passes information between them (http://www.cesm.ucar.edu/models/cesm1.1/cesm/doc/usersguide/x51.html). The control run was forced by the observed climatologically mean SST; the experimental run was forced by the observed SST in 2011. The model was integrated for 30 years at a resolution of 0.9° latitude by 1.25° longitude and a timestep of 30 minutes.

The seasonal influence of ENSO on geopotential thickness[7] anomalies and 500 hPa height anomalies in April is assessed using a lead-lag correlation between the nino3.4 index from November (5-month lead) to April (0-month lead or concurrent). We use geopotential height fields from MERRA (Rienecker et al., 2011) for the period 1979-2012. We use stepwise regression *[Hocking, 1976]* and Partial Least Squares Regression *[PLS, Tenenhause et al., 2005]* to investigate the role of SSTAs in the Pacific and the Atlantic on 500 hPa geopotential height anomalies over the South Central Unites States (domain: 24-40N and 110-92W). Stepwise and PLS regression can minimize the collinearity (if any) between the predictors. We use Nino3.4, Nino4, PDO and AMO indices from January (3-month lead) to April (0-month lead or concurrent) to assess the influence of these potential predictors on April 500 hPa height anomalies. We next use the same indices for May (1-month lead) and for June-to-August (JJA mean, concurrent) to assess their influence on mean JJA 500 hPa height anomalies. Stepwise regression selects the most important predictors to use in the regression model. Next, we use PLS to assess the total variance in the geopotential height anomaly attributable to the retained predictor indices.

Does surface dryness contribute to the mid-tropospheric ridge in the late-spring to early summer over the South Central US? To answer this question we undertook lead-lag correlation between pentad soil moisture anomalies and 500 hPa geopotential height anomalies for the period May to June. Soil moisture is from the North American Regional Reanalysis (NARR, Mesinger et al., 2006) 3-hourly column soil moisture content and the 500 hPa geopotential heights are from NCEP-CDAS1 daily data. Latitudinal means were removed in the 500 hPa height field prior to analysis. The two datasets were aggregated to pentads and deasonalized by removing the mean pentad value. Anomalies in both the soil moisture and geopotential height field were obtained by subtracting the time means from the datasets.

---

[7] Geopotential thickness measures the vertical distance, or thickness, between two pressure surfaces – typically between 1000 hPa and 500 hPa (i.e. land surface to mid-troposphere). The distance between two pressure levels is proportional to the mean air temperature between those two levels. High values thickness are associated with warm air and low values of thickness are associated with cold air. Geopotential thickness anomaly is a variable used to diagnose anomalous heating in the atmospheric column.

1.3: Evolution of drought over the Southern Plains

1.3.1: Drought onset

In September 2010, a rainfall deficit became apparent in eastern Texas and the southeast US (Fig. 1.1). By winter 2010/2011, dry conditions over the southern Plains intensified. In the spring of 2011, drought expanded westward to western Texas, and New Mexico. In June, drought reached D4 status over Texas, Oklahoma and New Mexico. The drought continued through November. In December, several rainfall events brought some relief to eastern Texas. Texas received above normal rainfall in the winter of 2011/2012. By March 2012, most of state, except west Texas, had recovered from the meteorological drought.

The La Niña event was established by the summer of 2010, as depicted by the negative SSTAs in the tropical Pacific Ocean (Fig. 1.2a). By September, the SSTAs in the Nino 3.4 region reached -1.5 C. The cold ENSO reached the maximum intensify in December 2010. Rainfall deficits over eastern Texas and the southeast US became well-established with anomalies dipping below -0.8 (Fig. 1.3e). The drought intensified over the winter of 2010/2011 (i.e. DJF 2010/2011). Negative rainfall anomalies started to shift westward in early-spring while the La Niña event was weakening. By the summer of 2011, ENSO had transitioned towards neutral conditions. However, there were positive SSTAs in the North Pacific and negative SSTAs along the West Coast of the United States. While ENSO reached neutral conditions, drought over Texas continued to intensify and reached D4 status throughout most of the state (Fig.1.3h).
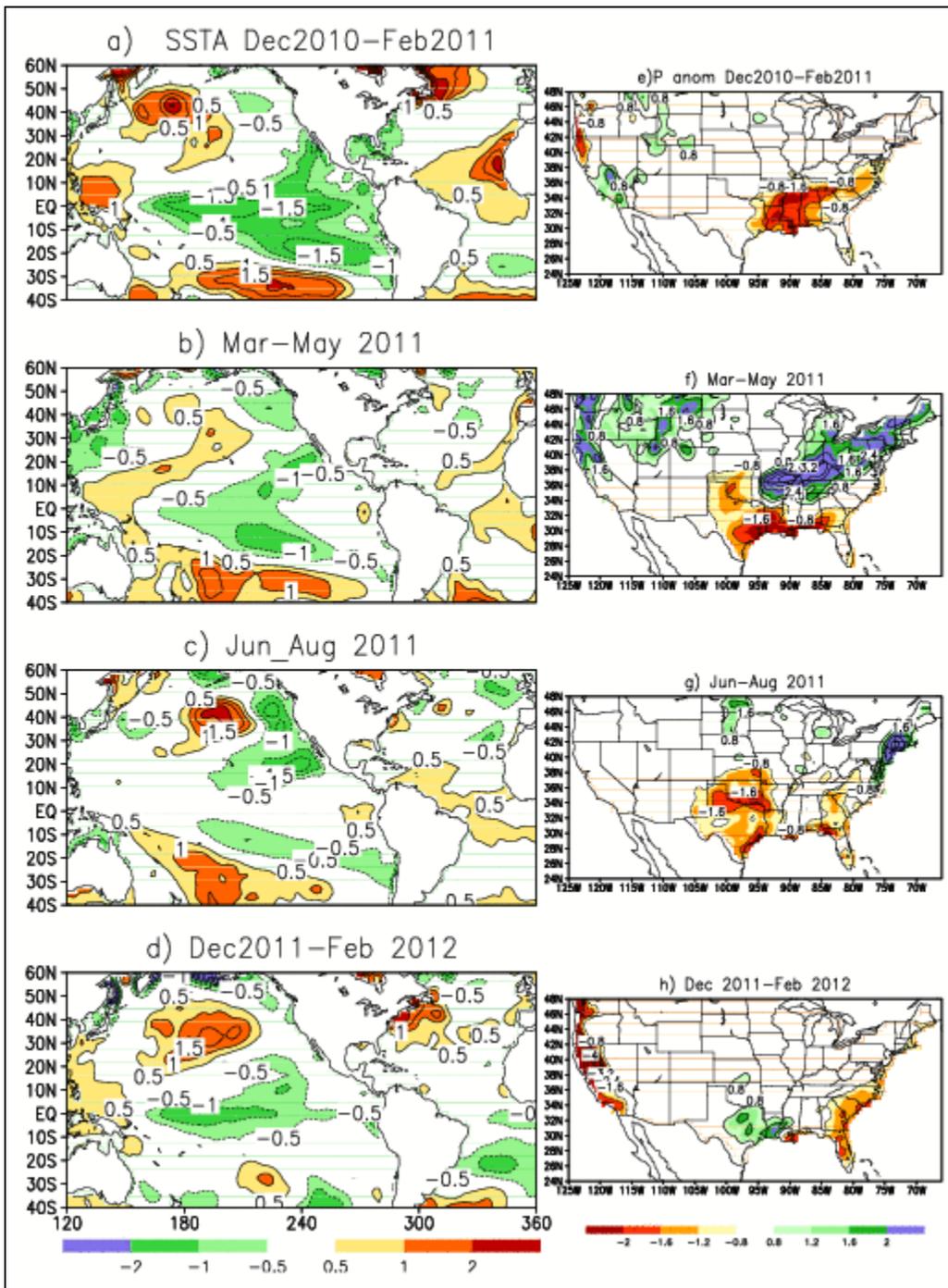
Figure 1.3: Seasonal SSTA anomalies in the Pacific and Atlantic ocean basins and associated precipitation anomalies over the United States in Dec 2010-Feb 2011 (a and e), Mar-May 2011 (b and f), Jun-Aug 2011 (c and g), and Dec 2011-Feb 2012 (d and h). Contour interval for SSTAs is 0.5°C. Contour interval for precipitation anomalies is 0.1 (unitless).

1.3.2: Drought intensification in spring and summer

La Niña's influence on spring atmospheric circulation anomalies

The 2010/2011 La Niña event established favourable conditions for dryness in the winter. During La Niña events a weakening and poleward displacement of the sub-tropical jet stream deflects winter storm tracks north of their climatological location and causes a reduction of precipitation over the southern Great Plains (Eichler and Higgins, 2006; Kousky and Ropelewski, 1989). We find that the sub-tropical jet stream (identified by zonal wind anomalies at 200 hPa) continued to be weaker and displaced poleward even in March and April 2011 [Fig. 1.4(a) and 1.4(b)] as depicted by positive 200 hPa zonal wind anomalies over the mid-latitudes (hence, a stronger jet stream over these regions) and negative 200 hPa zonal wind anomalies (indicating a weaker jet stream) over the southern regions of North America. Column thickness anomalies, defined as mean height anomalies from 1000-500 hPa with latitudinal means removed, from March to May 2011 show highly above normal thickness over the southwestern and south central regions in March and April 2011 [Fig. 1.4(a) and 1.4(b)] indicating the extension of anomalous warmth from the surface to the mid-troposphere. In May 2011, the jet stream curves over the south central regions and there is a decline in positive thickness anomalies. Above normal warmth is concentrated over south Texas and northern Mexico in May 2011 [Fig. 1.4(c)].

Above-normal thickness over the southwestern and south central regions in March and April 2011 would drive a west-east gradient in geopotential height influencing zonal circulation. We find that the anomalous westerly wind at 850 hPa over Texas was more than twice its climatological strength from March to May 2011, with a burst of very strong westerly winds in late-April [Fig. 1.5(e), red bars]. Furthermore, the transition from westerly to easterly winds at 850 hPa was delayed to early June compared to the climatological transition point of early-May [Fig.1.5(e), solid black line]. The April 850 hPa zonal wind anomaly over Texas in April 2011 was the strongest since 1951 (Fig. 1.6).
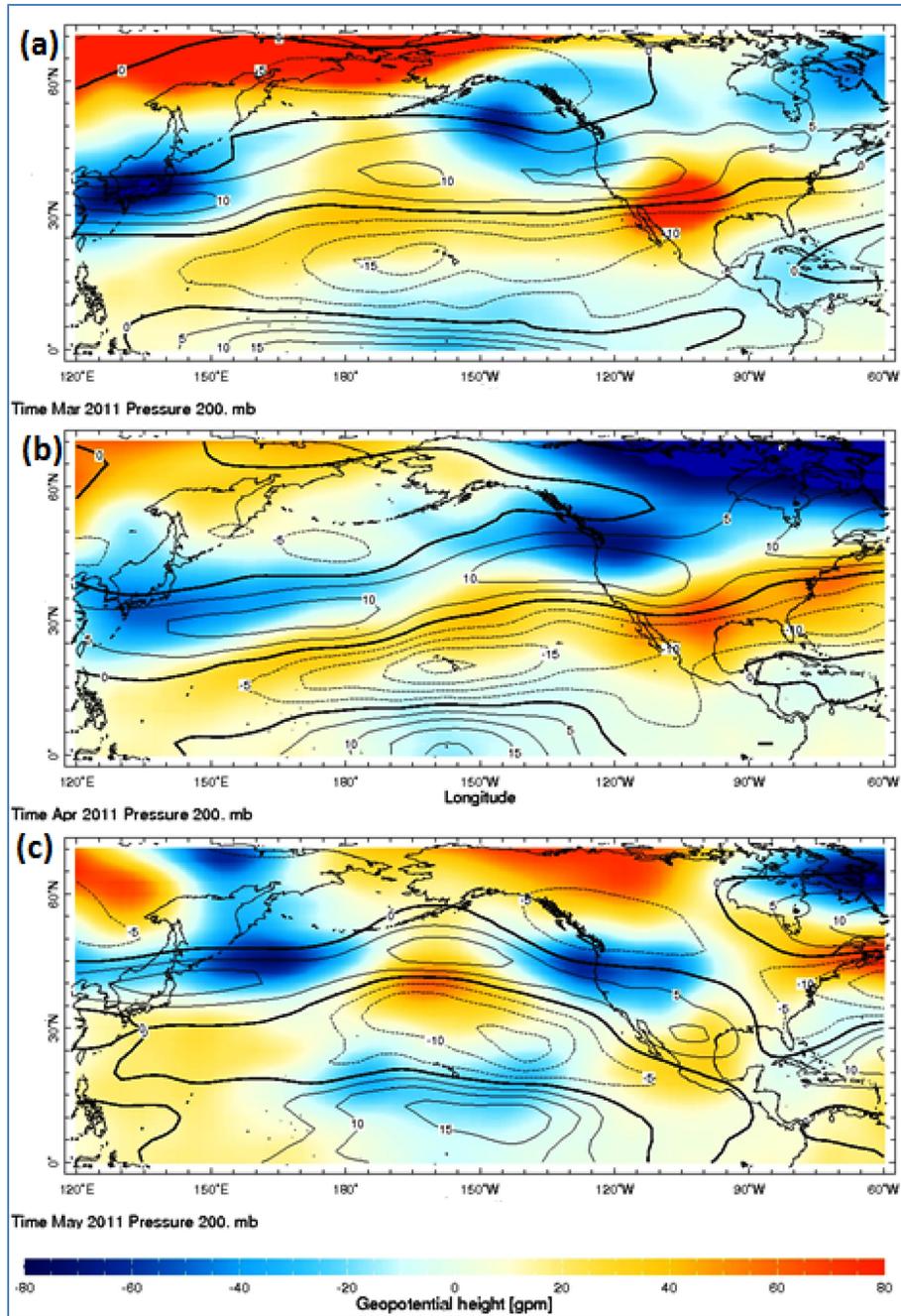
Figure 1.4: (a) Jet stream anomalies (depicted by 200 hPa geopotential height anomalies) superimposed on 1000-500 hPa thickness anomalies with latitudinal means removed for March 2011. Contour interval for 200 hPa height anomalies is 5m and shading contours for column thickness is 20m. (b) same as (a) but for April 2011. (c) same as (b) but for May 2011.

Does La Niña cause the strengthening of U850 in April? Observations indicate a sharp west-east geopotential height gradient between 125W and 104W [Fig. 1.7(a)]. Experimental runs of the CESM 1.1.1 model, forced with 2011 SSTAs (that includes the strong La Nina event of 2010/2011), show a strengthening of the geopotential height gradient in April compared to control runs (derived from a 30-year climatology) [Fig. 1.7(b)]. Such a gradient would drive an increase in lower-tropospheric zonal winds – particularly at the 850-700 hPa levels. Zonal wind anomalies from the experimental runs also show above normal westerlies in April 2011 [Fig. 1.7(d)]. These results imply the key role that 2011 SSTAs played in driving the enhanced west-east geopotential height gradient and the strengthened westerlies at 850 hPa over Texas in the late-spring.

Historically, about 11% of La Niña-induced winter droughts over Texas ended in spring (Annex 1). Those that persisted through spring tended to develop into severe, as indicated by the Palmer Drought Severity Index ($-3 \leq PDSI \leq -2$), to extreme droughts ($PDSI \leq -3$) in summer. Anomalously strong westerlies at 850 hPa (U850) in April is a characteristic feature of all 7 severe-to-extreme drought events, from 1951 to the present (i.e. 1951, 1954, 1955, 1956, 1963, 2006 and 2011), that had persistent negative rainfall anomalies from winter through summer.

Role of convective inhibition in drought intensification

Large negative values of CIN [Fig. 1.5 (a), thick red line] started to develop in late April and early May and continued through the summer of 2011. Negative CIN during spring and summer is a common feature in the other three strongest drought events of the last century – i.e.1917/18, 1924/25 and 1955/56 – as shown by the thick yellow line in Fig. 1.5(a). However, the magnitude of the negative CIN value from late-spring to early summer in 2011 was even stronger than that observed in these past extreme droughts.

An increase of CIN can be caused by a decrease of surface relative humidity or increase in dewpoint depression (T_d), and by an increase of temperature in the lower troposphere that leads to a more stable temperature stratification. We find that temperature at the surface (T_{surf}) and 850 hPa (T_{850hPa}) increased steadily from March through June [Fig. 1.5(b)] and continued through summer. While the increase in temperature in March through June is to be expected with the transition of the seasons, T_{surf} and T_{850hPa} in 2011 were both anomalously higher than climatology [Fig. 1.5(b)] in late-February, early-March, and late-April through August. T_{surf}, T_{850hPa} and T_d [Fig. 1.5(c)] show a sharp increase from mid-April to mid-May, coincident with sharp increases of CIN and 500 hPa heights [Fig. 1.5(d)]. T_d was anomalously high from end-April through early-June and then follows climatological values for the rest of June. From July through August T_d steadily increases and is anomalously high indicating very dry soil moisture conditions in the late-summer of 2011. The enhanced geopotential gradient could be instrumental in the eastward advection of temperature. This probably explains the sudden increase in T_{surf}, T_{850Pa}, CIN and 500 hPa heights in late-April and early-May over Texas.
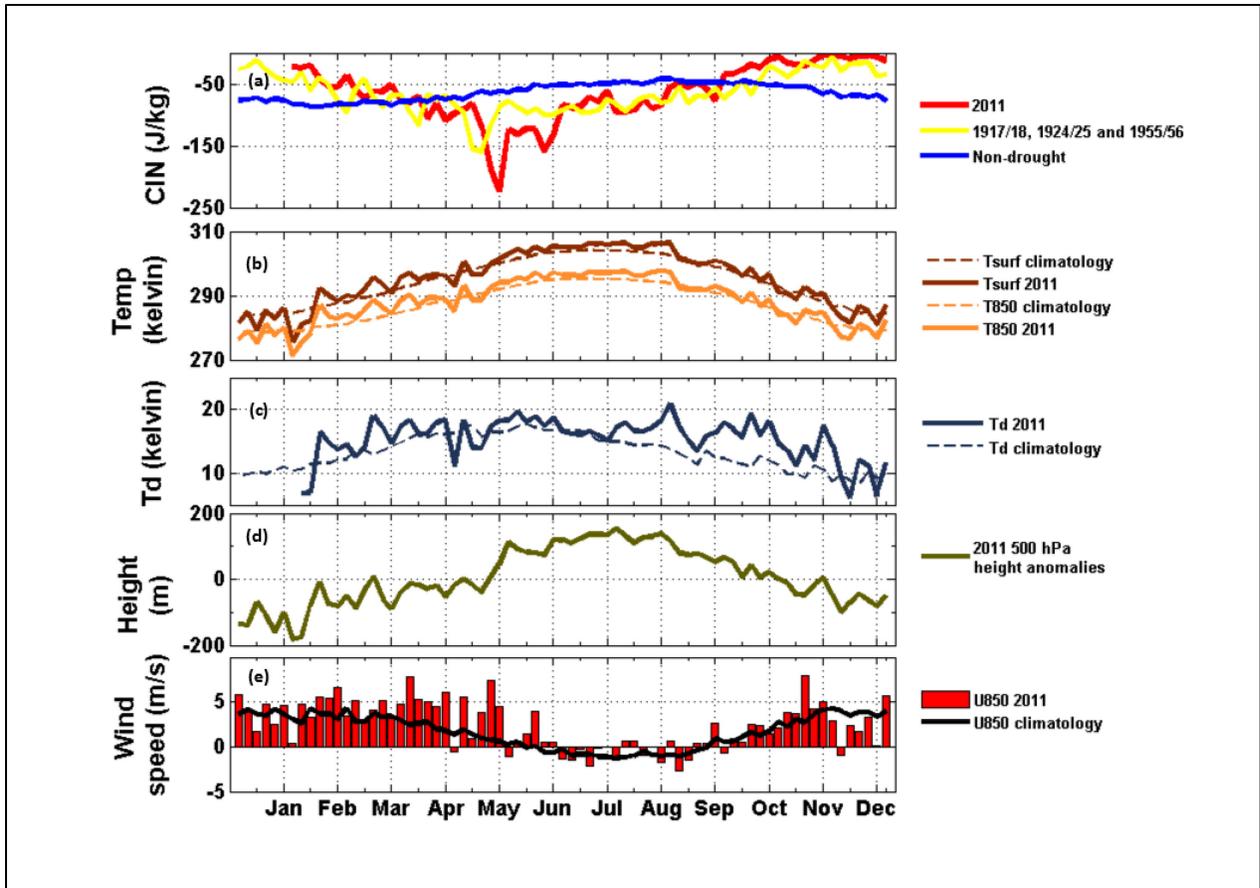
Figure 1.5: (a) Pentad (5-day) values of convective inhibition (CIN) for February-December 2011 (red), mean for drought years of 1918, 1925 and 1955 (yellow), and non-drought (blue); (b) area-averaged pentadal surface temperature (solid maroon line) and climatology (dashed maroon line) and temperature at 850 hPa (solid orange line) and climatology (dashed orange line) ; (c) area-averaged pentadal dewpoint depression (Td) for 2011 (solid dark blue line) and climatology (dashed dark blue line); (d)area-averaged pentadal 500 hPa height anomalies; and (e) area-averaged pentadal zonal wind at 850hPa for 2011 (red bars) and climatology (black line)
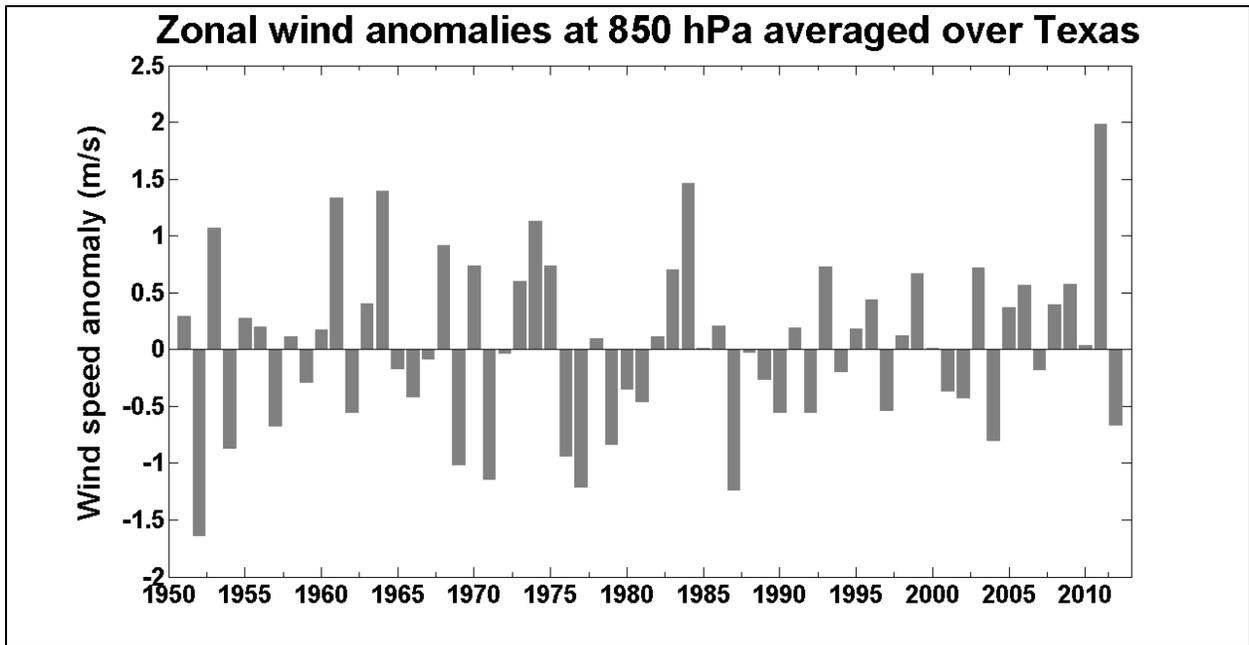
Figure 1.6: Zonal wind anomalies at 850 hPa averaged over the domain of Texas (25-38N and 108-93.5W).
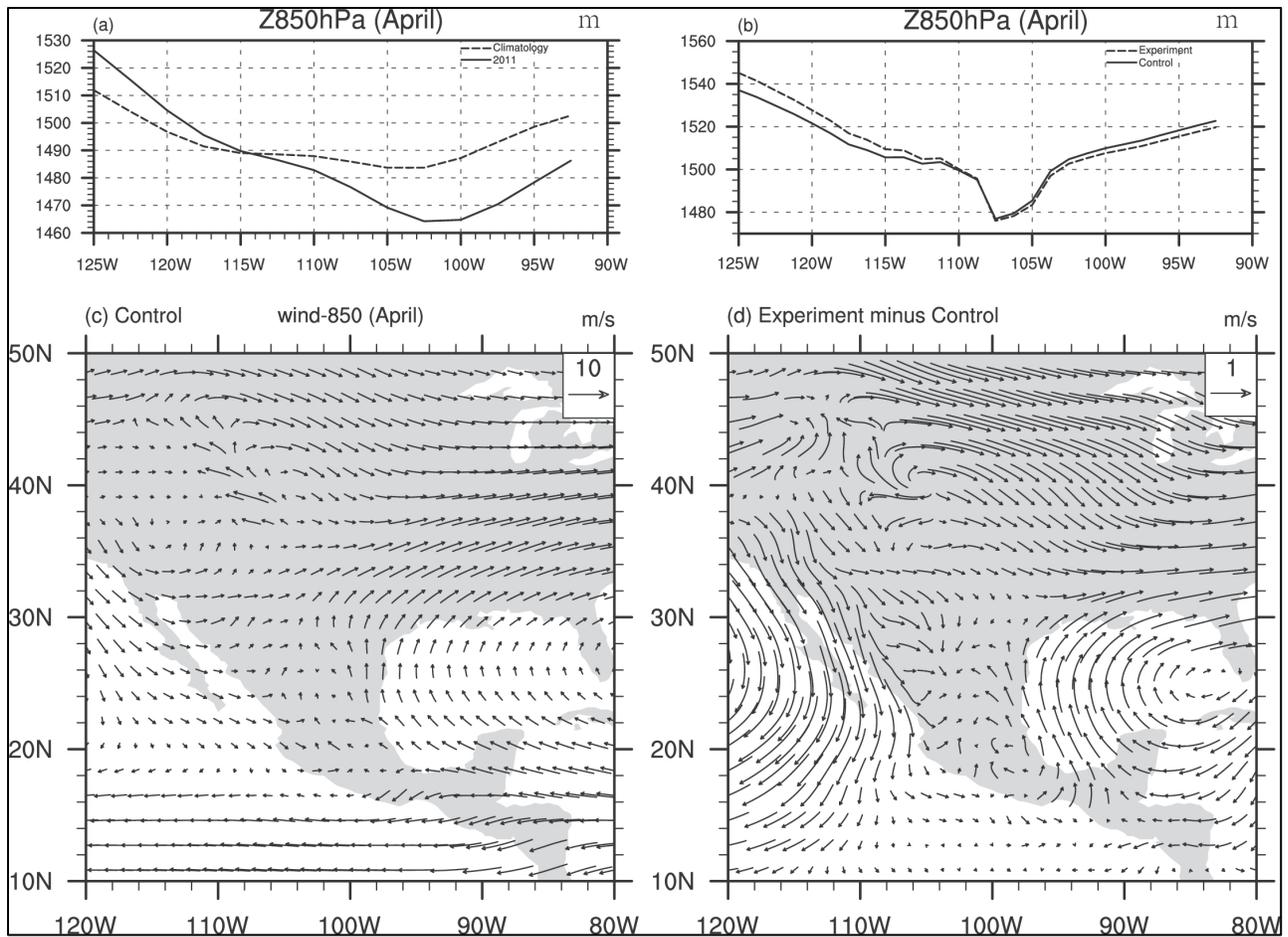
Figure 1.7: (a) Observed April 2011 (solid black) and climatological (dashed grey) west-east geopotential gradient from 125W-90W over the South Central US ; (b) April west-east geopotential gradient from control run (solid black) and from experiment (dashed black) forced with 2011 SSTAs)and (c) April U850 from control and (d) experiment minus control April U850.

Role of SSTAs versus land surface conditions in setting up the mid-tropospheric ridge in the late-spring/early-summer

SSTAs

What drives the mid-tropospheric ridge over Texas, which is a common characteristic during extreme summer droughts? We first examine the role of SSTAs on the 500 hPa geopotential height anomaly field to ascertain the role of SSTAs in different ocean basins. Given the established influence of ENSO on the sub-tropical jet stream and, hence, rainfall over the South Central US, we first study the lagged correlation between the Nino3.4 index and observed 500 hPa height anomalies from November through April. We find that there is a statistically significant negative correlation (blue shading) extending from the central eastern Pacific to south central regions of North America at the 3-month (January) to 0-month (April, or contemporaneous) time lags [Figs. 1.8(b) to 1.8(d)]. This implies that cold (warm) tropical Pacific SSTAs drive mid-tropospheric stability (instability) – and, hence, lower-tropospheric warming (cooling) – in April from the 3-month to the contemporaneous time lag. Lower-tropospheric warming would lead to an increase in the east-west temperature gradient over the southern US and, hence, strengthened U850.

Is La Niña alone responsible for mid-tropospheric stability in the spring and the summer? Stepwise regression between lagged[8] and simultaneous SSTAs in the tropical and central Pacific, north Pacific and Atlantic with geopotential height anomalies in April shows that at the 3-month lag (i.e. January), SSTAs in the central Pacific (i.e. Nino4) and the north Atlantic (i.e. AMO) are the only viable predictors, with the former explaining 47% and the latter explaining 19.7% of the variance in the anomalous 500 hPa height field (Table 1.1). At the 2-month lag, SSTAs in the central Pacific, north Pacific (i.e. PDO) and north Atlantic are the viable predictors explaining 32%, 24% and 5% of the variance in the anomalous 500 hPa height field respectively. At the 1-month lag (i.e. March), SSTAs in the north Pacific and north Atlantic account for 8% and 32% of the variance in the anomalous 500 hPa height field. At the simultaneous time scale (i.e. April), SSTAs in the central Pacific and north Atlantic account for 38% and 15% of the variance in the anomalous 500 hPa height field. This implies that mid-tropospheric stability over Texas in the spring is driven by SSTAs in both the central and north Pacific and the north Atlantic. Variance in the anomalous 500 hPa height field in the summer months of JJA at the 1-month lag (i.e. May) can be attributed primarily to SSTAs in the central Pacific, with Nino4 accounting for 39.6% of the variance (Table 2). The PDO and AMO account for 4% and 6% of variance in the height field. At the simultaneous time lag (i.e. JJA), the only viable predictors are SSTAs in the north Pacific and the north Atlantic. However, these account for only 8% and 2% of the total variance in the anomalous JJA height

---

[8] Shifting of viable predictors by different lag times is undertaken to assess which lead times have potential skill with respect to forecasting mid-tropospheric stability using SSTAs.

The climate system can have such a large (e.g. 3-month) memory due to the large heat capacity of the ocean. While short and medium-range weather forecasts require accurate observations of initial atmospheric states, at the seasonal timescale (e.g. 3-month) the importance of initial conditions weakens (Goddard et al., 2001) as detailed memory of initial atmospheric conditions is lost. Therefore, seasonal climate prediction depends on detailed changes in boundary conditions. SSTs are surface boundary conditions that govern the convergence of moisture flux and sensible and latent heat fluxes between the ocean and atmosphere (Shukla and Kinter, 2006). The surface boundary layer has a relatively longer time scale of variability and thus allows for predictability that extends to the seasonal time scale – i.e. a few months. Such an extended range of predictability is believed to exist due to atmospheric-oceanic-land coupling (Palmer, 1993).

field (Table 1.2). This implies either that simultaneous SSTAs are probably only very weakly responsible for, or that they have a non-linear impact on, the mid-tropospheric height anomaly clearly evident during extreme drought events over the south central region. It could also imply the probable role for land surface feedback in the strengthening and persistence of the mid-tropospheric height anomaly over the summer months.
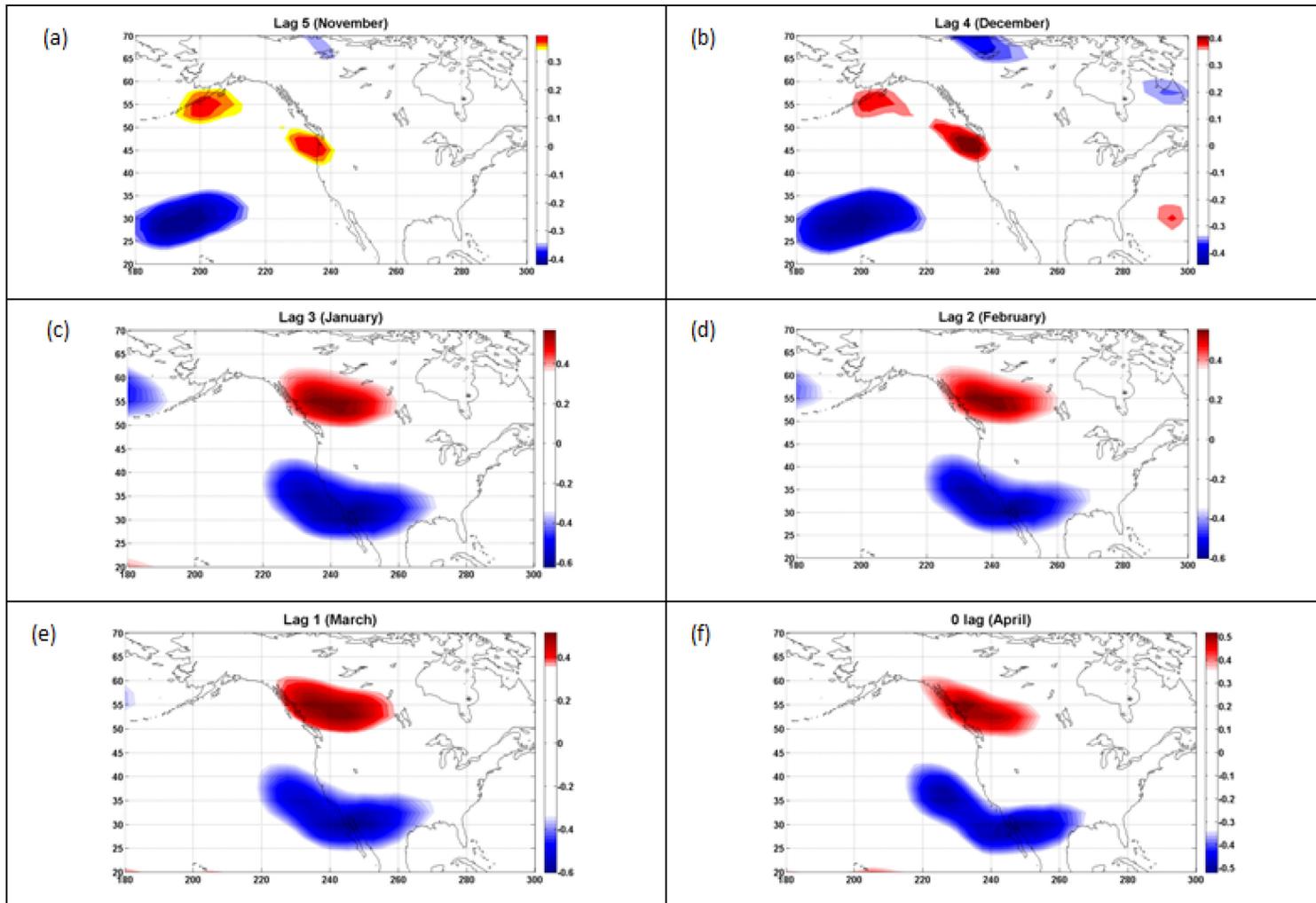
Figure 1.8: (a) Lag 5-month (November) correlation of Nino3.4 with April 500 hPa geopotential height anomalies. Contour shading interval is 0.1. Latitudinal means have been removed in the geopotential height anomaly field; (b) same as (a) but for lag 4-month (December); (c) same as (b) but for lag 3-month (January); (d) same as (c) but for lag 2-month (February); (e) same as (d) but for lag 1-month (March); and (d) same as (e) but for lag 0-month (April).

Table 1.1: Correlation between lagged and simultaneous predictor variables retained by stepwise regression and April z500 anomalies, variance in April z500 anomaly field explained by each predictor variable, and predicted z500 anomaly for April 2011.

Lag (month)	January		
Variable retained	Nino4	AMO	
Variance explained	47%	19.7%	
Correlation value	0.82		
Predicted z500 anomaly	0.77		

Lag (month)	February		
Variable retained	Nino4	PDO	AMO
Variance explained	32%	24%	5%
Correlation value	0.78		
Predicted z500 anomaly	0.01		

Lag (month)	March		
Variable retained	PDO	AMO	
Variance explained	8%	32%	
Correlation value	0.64		
Predicted z500 anomaly	0.65		

Lag (month)	April (simultaneous)		
Variable retained	Nino4	AMO	
Variance explained	38	15%	
Correlation value	0.73		
Predicted z500 anomaly	0.56		

Table 1.2: Correlation between lagged and simultaneous predictor variables retained by stepwise regression and mean JJA z500 anomalies, variance in mean JJA z500 anomaly field explained by each predictor variable, and predicted mean z500 anomaly for JJA 2011.

Lag (month)	**May**		
Variable retained	Nino4	PDO	AMO
Variance explained	39.6%	4%	6%
Correlation value	0.70		
Predicted z500 anomaly	0.06		

Lag (month)	**JJA (simultaneous)**	
Variable retained	PDO	AMO
Variance explained	8%	2%
Correlation value	0.32	
Predicted z500 anomaly	-0.06	

Land surface conditions:

The lead-lag correlation between MJJ soil moisture anomalies and MJJ 500 hPa geopotential height anomalies depicts a statistically significant positive correlation at negative 6 lags (Fig. 1.9). This indicates that soil moisture anomalies typically lead an increase in 500 hPa geopotential height by 30 days or approximately 1 month. The positive correlation diminishes steadily with subsequent pentads and switches to negative correlation around positive 1 lag. The correlation is no longer significant. Spring dryness usually follows from cumulative soil moisture deficits resulting from deficit precipitation from winter through spring. The lead-lag correlation result appears to indicate that spring dryness contributes to establishing the ridge at 500 hPa in the summer and highlights the importance of land surface feedback as a driver in drought persistence from spring through summer. In 2011, we see that the drought was established in the spring with soil moisture anomalies over Texas being in the 10th percentile [Fig. 1.10(a), orange shading]. By the summer the mean soil moisture percentiles had dropped to the 5th percentile [Fig. 1.10(a), red shading'. The soil moisture deficit continued until December 2011. Meanwhile, evapotranspiration (E) also decreased during the drought because of the lack of soil moisture [Fig. 1.10 (b)] over Texas, Oklahoma and eastern New Mexico. This means there was less latent heating. The radiation terms were not influenced by the drought, so the lack of E was balanced by positive sensible heat anomalies [Fig. 1.10(c)], which increased surface temperature anomalies in JJA. The surface temperature anomalies are $4^{o}C$ above normal in JJA [Fig. 1.10(d)]. The high temperature is consistent with the anticyclonic circulation over the Southern Plains (Fig. 1.11). This results in the westward displacement of the vertically integrated moisture transport (Fig. 1.11, colored) and strong easterlies at the lower level (i.e. 850 hPa). There is less moisture transported from the Gulf of Mexico to the Southern Plains which means less rain. The feedback loop intensifies the drought impact, thus contributing to the maintenance of drought in the summer. The lead-lag correlation result and the observed reduction in JJA rainfall in 2011 corroborates an observational study by Zhang et al. (2008b), which highlights the south central and northwestern US as regions with statistically significant 1-month lead correlation between May-to-July soil moisture and June-to-August evapotranspiration, implying a strong control by soil moisture on evapotranspiration.
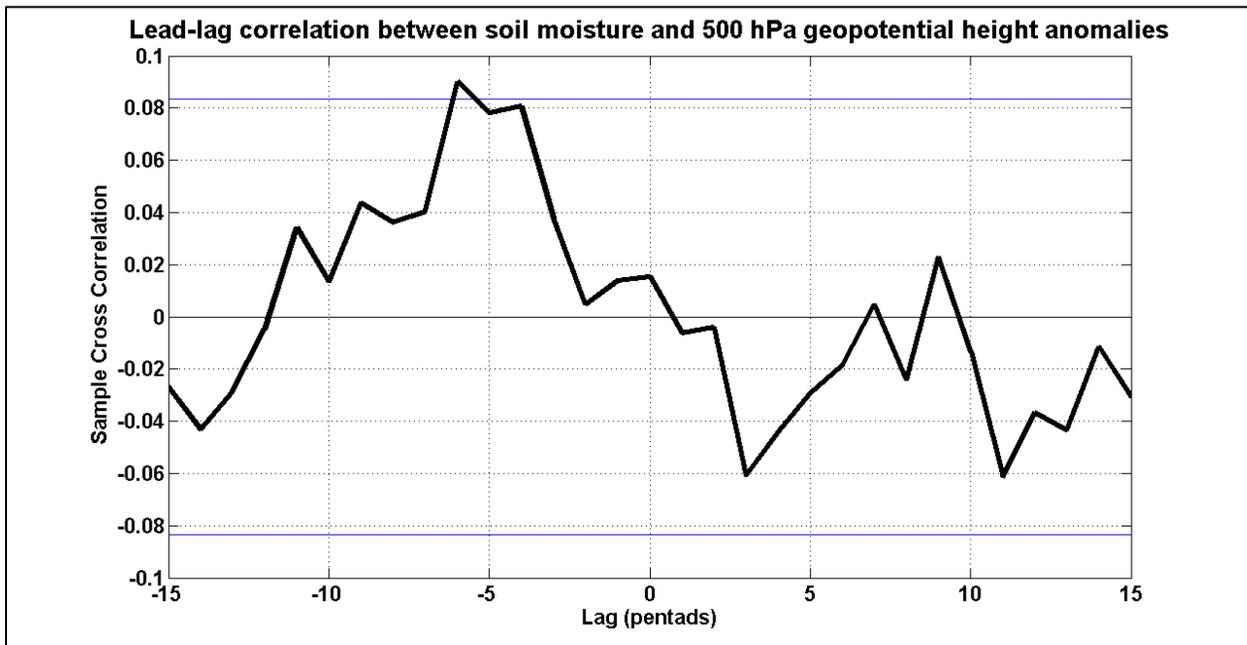
Figure 1.9: Lead-lag correlation (solid black line) between May-to-June (MJJ) soil moisture anomalies and MJJ 500 hPa geopotential height anomalies over Texas. Lags are in pentads. Upper and lower 95% confidence bounds are depicted as blue horizontal lines.
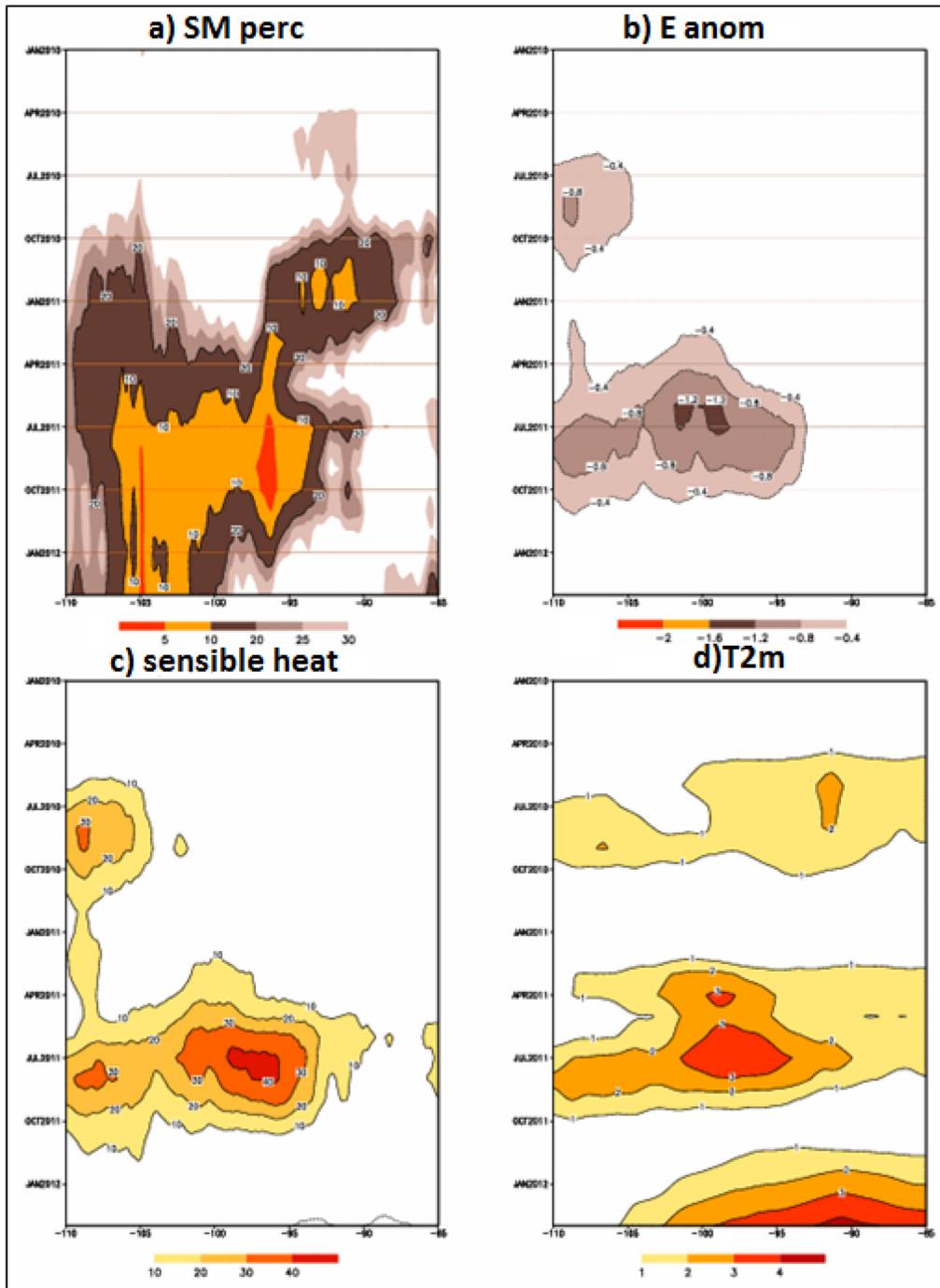
Figure 1.10: (a) Time-longitude plot for soil moisture percentiles, with contour interval of 5 percentiles, (b) same as (a) but for evaporation anomalies with contour interval of 0.1mm/day, (c) same as (b) but for sensible heat anomalies, with contour interval of 10 wm^{-2}, and (d) same as (c) but for 2-meter (T2m) temperature anomalies, with contour interval of 2°C.
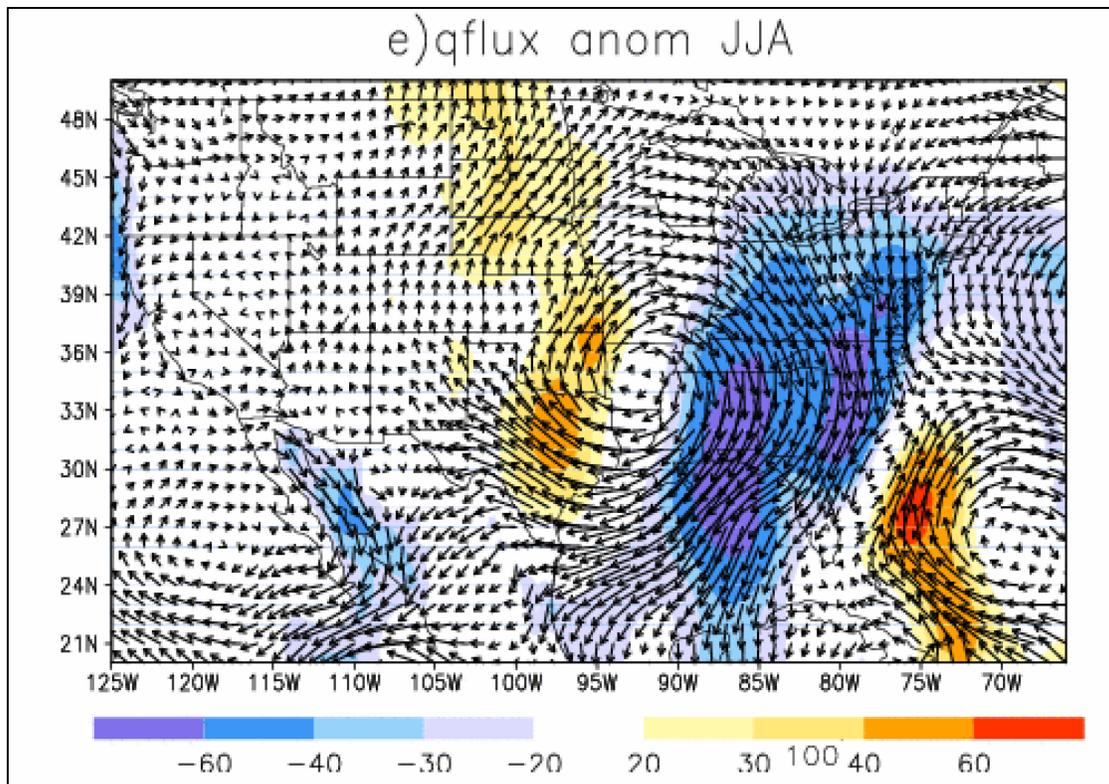
Figure 1.11: Vertically integrated moisture transport (qflux) anomalies (contour interval is 10mm/day) and mean wind vector at 850 hPa in JJA 2011.

Role of North Pacific SSTAs on summer drought intensification

In addition to land surface conditions being conducive for drought intensification in the summer, North Pacific SSTAs were also probably responsible for a decline in total JJA rainfall. In JJA 2011, there were positive SSTAs in the North Pacific and negative SSTAs along the west coast of the United States [Fig. 1.3(c)]. This pattern of North Pacific SSTAs has large negative projection on the Pacific Decadal Oscillation mode. The JJA averaged PDO time series from 1915 to 2010 is shown in Fig. 1.12(a). The negative phase of the PDO favors dry conditions (depicted by negative values of the SPI6 in August) in the summer over the US southwest and Texas [Fig. 1.12(b)].
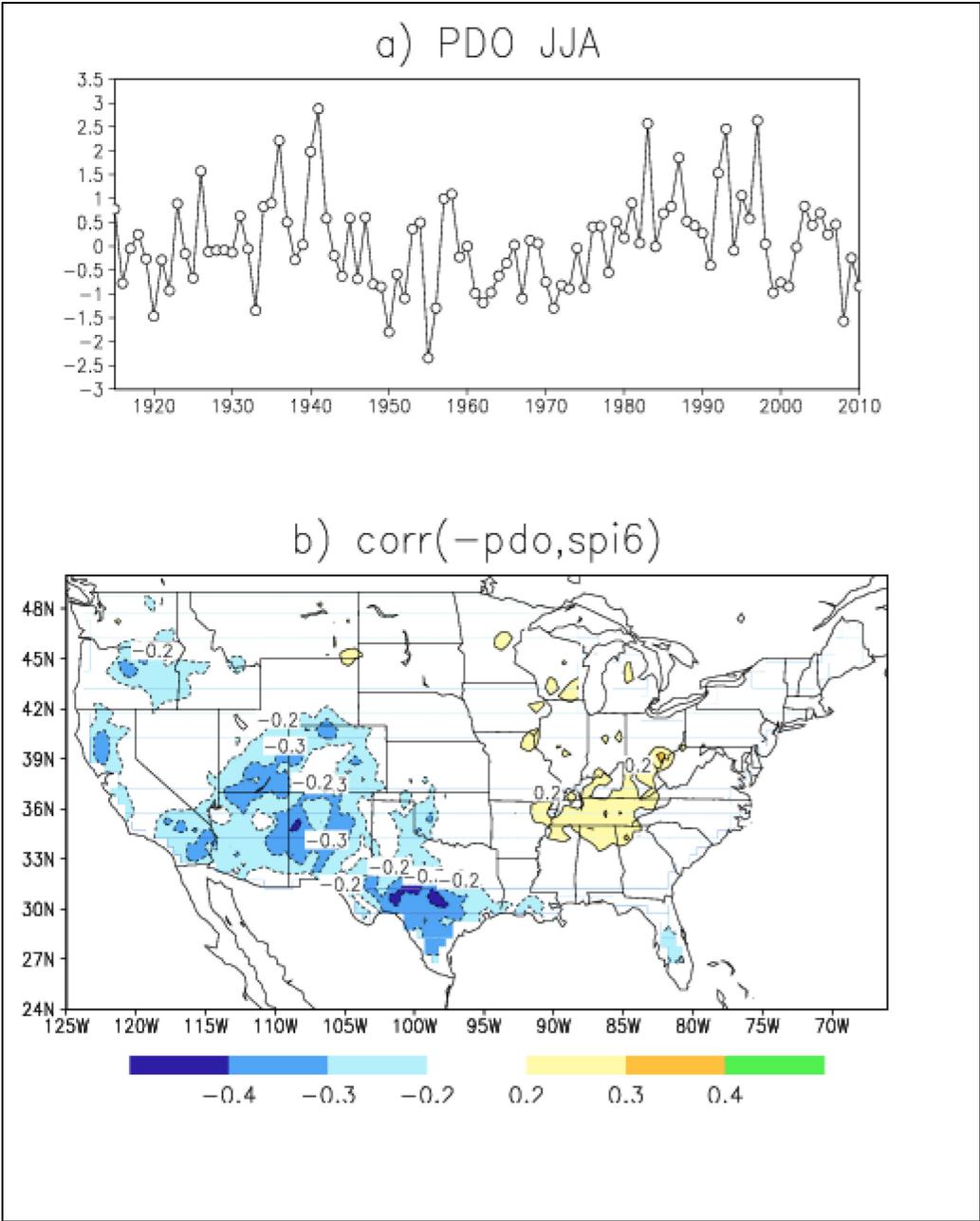
Figure 1.12: (a) Mean PDO time series for JJA from 1915-2010, and (b) the correlation between mean JJA PDO and SPI6. Correlation contour interval is 0.1. Only correlation values significant at the 95% confidence level are shown.

1.3.3: Demise of the drought

Drought demise occurred in the winter of 2011/2012 [Fig. 1.3(h)], despite a second La Niña event that set in during the fall of 2011 and continued until February 2012 [Fig. 1.2(b), green shading at lower end of plot]. What was the forcing responsible for the demise of the drought?

A comparison between the winter SSTAs for 2010/2011 and 2011/2012 shows the possible causes. In the tropical Pacific, SSTAs for both years show a La Niña pattern with negative SSTAs less than -1°C in the tropical Pacific and positive SSTAs in the North Pacific. The largest differences are in the North Atlantic. For DJF 2010/2011, there were positive SSTAs in the tropical Atlantic and in the high latitudes north of 55°N with negative SSTAs along the Atlantic coast [Fig. 1.13(a)]. This pattern will have a large positive projection onto AMO. A positive phase of the AMO will enhance the impact of La Niña events on precipitation over the southern United States (*Mo et al.* 2009, *Shubert et al.* 2009). That may explain the intense dry conditions over the Southeast and the eastern Texas in 2011.

The situation for DJF 2011/2012 was different. There were strong positive anomalies over the North Atlantic near the east coast of the United States [Figs. 1.13(d)]. The precipitation anomalies are below normal over the Southeast, but above normal over the eastern Texas [(Fig. 1.3(h)].

For the 2010/2011 winter, the North Atlantic Oscillation (NAO) was in a negative phase. This is evident from the 850 hPa height anomalies (Z850) for DJF 2010/2011 [Fig. 1.13(b)]. It has negative height anomalies in the Atlantic with positive heights to the north which is consistent with negative SSTAs along the Atlantic coast of the United States and positive SSTAs to the North. The 850 hPa wind anomalies, consistent with the height anomalies, show cyclonic circulation anomalies from the eastern United States to the Atlantic centered along 40°N and anti-cyclonic wind anomalies to the north and south. The negative anomalies over the eastern United States are responsible for a weaker low-level meridional wind from the Gulf of Mexico to the central United States. Therefore, there was less moisture from the Gulf to the Southern Plains and less rainfall for 2011.

For the DJF 2011/2012 season, weak positive anomalies were located in the Atlantic centered at 35-40° N, while negative anomalies were in the North Atlantic in October-November 2011 [Fig. 1.13(d)]. For 2011/2012 winter, the NAO is in the positive phase and the 850 height anomalies show positive anomalies in the North Atlantic with negative anomalies to the North which is consistent with positive SSTAs in the North Atlantic centered at 40°N. The 850 hPa wind anomalies show anti-cyclonic circulation anomalies in the Atlantic. This is consistent with the positive phase of the NAO. The anti-cyclonic circulation implies stronger than normal low-level meridional wind. There was a stronger moisture transport from the Gulf of Mexico to the central United States. Therefore, there was more rain over the southern Plains.
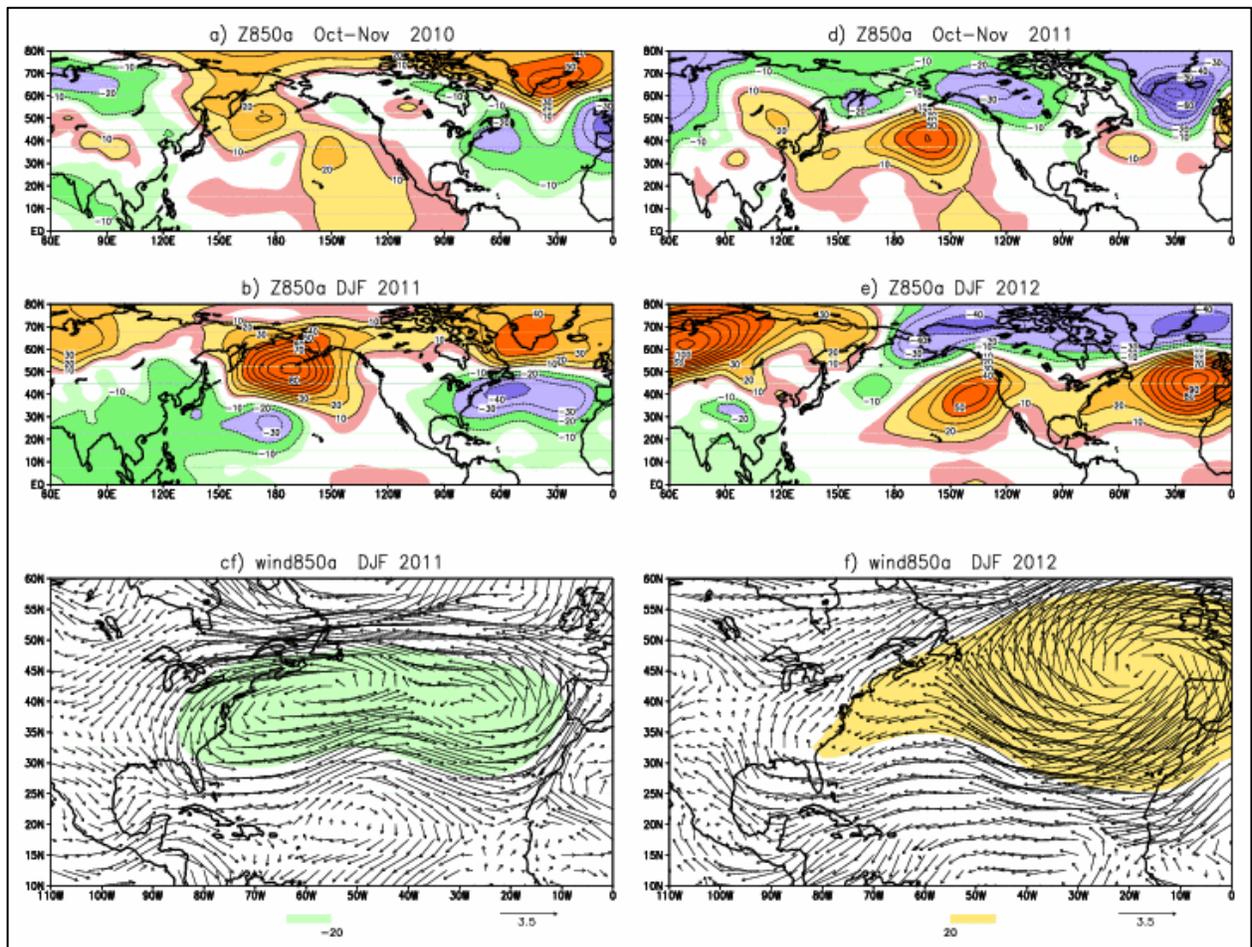
Figure 1.13: (a) 850 hPa height anomalies for Oct-Nov 2010. Contour interval is 10m. Contours -5 and 5 m are added. Zero contours are omitted. (b) same as (a), but for the DJF 2011 mean, (c) 850 hPa wind anomalies for DJF 2011 super imposed on the 850 hPa height anomalies less than 20m are colored. The unit vector is 3.5 ms^{-1}. (d)-(e) same as (a)-(b) but for 2012 and (f) same as (c). 850 hPa height anomalies more than 20 m are colored.

4. Conclusions

The recent drought over Texas was one of strongest drought events in this century. It lasted more than one year from October 2010 to December 2011 and spread beyond Texas to Oklahoma, Kansas, New Mexico and Louisiana. This paper reviews the evolution of the drought event and examines the physical mechanisms and forcing responsible for the drought.

The trigger of drought was the La Niña event that was established one season before the rainfall deficit made an appearance over the southern plains. In 2010/2011 winter, a negative NAO was in the Atlantic. The circulation anomalies influenced by La Niña and the negative NAO were in favor of a three cell pattern of SSTAs with negative SSTAs in the North Atlantic along 40^oN and positive SSTAs to the north and south. The cyclonic circulation associated with the height anomalies over the eastern United States was in favor of a weaker low-level meridional wind. Less moisture transported into the southern plains resulted in a dryer Texas.

The anomalous warmth in the spring over the south western and south central United States can be attributed to the influence of SSTAs in the central and North Pacific and the North Atlantic in establishing the mid-tropospheric high pressure system over the region in April. Such anomalous warmth was instrumental in establishing a strong east-west temperature gradient over the southern United States that propelled a strengthening of the westerly zonal winds at 850 hPa and delayed the seasonal transition of westerlies to south easterlies in the late-spring. Experimental runs forced with 2011 SSTAs also indicate a strengthened east-west temperature gradient over the southern US and enhanced zonal winds at 850 hPa.

Anomalous westerlies at 850 hPa provided the trigger for the spring intensification of the 2011 drought by advecting warm dry air and anti-cyclonic vorticity over Texas. This established a highly stable environment in late-April and early-May, right at the beginning of the main rainfall season. The strengthening of the westerly winds at 850 hPa in late-spring is a characteristic feature in 7 severe-to-extreme droughts, experienced over Texas since 1951 that had persistence negative rainfall anomalies from winter through summer.

Precipitation deficits established in the winter of 2010/2011 intensified in April at the height of the rainfall season over Texas and peaked over the summer of 2011. Soil moisture decreased steadily with precipitation deficits from winter through spring. The reduction in soil moisture resulted in a decrease in evapotranspiration. To balance the negative latent heat anomalies, there was an increase of sensible heat which increased surface temperature anomalies over the southern plains. Soil moisture deficits in spring lead the establishment of a mid-tropospheric high pressure system by 30 days (~1 month). This indicates the potential role for land surface feedback on establishing the mid-tropospheric ridge over the south central US in extreme drought years. High temperature and associated anti-cyclonic circulation characteristic of a mid-tropospheric ridge further increases the stability of the atmosphere and leads to less rainfall, further strengthening the ridge later in the summer.

In the summer of 2011, there were positive SSTAs located in the North Pacific and negative SSTAs along the west coast of the United States. This pattern has a strong positive projection onto the Pacific Decadal Oscillation, which is known to drive a reduction in summer precipitation over Texas. Therefore, drought persistence in the summer of 2011 can be attributed to both land surface feedback stemming from the cumulative precipitation deficit from winter through spring and associated soil moisture-temperature-rainfall feedbacks and to SSTAs in the North Pacific.

Drought demise occurred in the winter of 2011/2012 even though a second La Niña event had set in during the fall of 2011, which continued until February 2012. In the 2011/2012 winter, the NAO was in its positive phase, with circulation anomalies favoring positive SSTAs in the Atlantic. The anti-cyclonic circulation anomalies also were in favor of a stronger meridional wind. There was more moisture transported into the southern plains resulting in more rainfall. Above normal winter rainfall helped relieved the drought over most of Texas.

Drought predictability to date relies primarily on ENSO-based predictability. We show that soil moisture feedbacks and atmospheric circulation such as the NAO can either amplify or dampen the ENSO influence. The influence of NAO on drought highlights the intrinsic limit of drought prediction.

This study identifies strengthened westerlies in the spring, North Pacific SSTAs and soil moisture feedback in the summer as key processes in drought intensification and persistence. It demonstrates how the anomalous circulation features in the spring are linked to large-scale circulation patterns in the winter and spring influenced by La Niña. These findings represent an important step forward in determining the causes and predictability of severe-to-exceptional droughts over Texas. The result also underscores the need for improved and continuous monitoring of soil moisture from winter through spring to assess the risk of summer drought intensification and persistence.

Part 2: Assessing Future Changes of Climate, Extreme Temperature and Drought over the South-Central United States Projected by the CMIP5 Models[9]

2.1: Introduction

The worst single year drought over the south central US in 2011, and the worst drought in 60 years that a large fraction of the US has experienced in 2012 are vivid reminders of the vulnerability of our society to droughts. To improve drought resilience, regional decision makers need to know whether and how climate will change, especially whether the statistical characteristics of droughts and surface temperature and rainfall will change, in the future. The climate projections by the Climate Model Intercomparison Project, Phase 5 (CMIP5) modeling groups and their downscaled products provide key information for regional decision makers. However, large inter-model discrepancies and apparent disagreements with observed changes during the past century over this region have so far largely prevented regional stakeholders from incorporating climate projections into their planning activities.

The climate community has done extensive research to assess future climate change and the underlying mechanisms driving climate over the southwest and southeast US and the US Great Plains (e.g., Seager et al. 2007, Cook et al. 2008; Li et al. 2011), using the Coupled Model Intercomparison Project Phase-3 (CMIP3) model outputs. However, few studies have focused on future climate changes over the SC US. Consequently, regional stakeholders only have access to studies that primarily focus on the SW US and the Great Plains (e.g., Seager et al. 2007; Karl et al. 2009). Recently, several studies have assessed future climate changes over Texas using CMIP3 models' outputs (Mishra and Singh 2009; Jiang and Yang 2012). However, the reliability of climate projections for this region has not been investigated thoroughly.

Previous studies have shown that droughts over the US Great Plains are mainly initiated by negative ENSO induced large-scale circulation anomalies in late fall and winter, with anomalously high geopotential or anticyclonic circulation centered over the western and central US (Wallace or Gutzler, 1981, Lyon and Dole, 1995; Mo et al., 1991, Trenberth et al., 1988). Such anomalous centers shift synoptic weather disturbances away from the Great Plains and central US, leading to a reduction of rainfall and facilitation of droughts, especially in winter and early spring. The anomalous mid-tropospheric high established in spring tends to persist through summer (Namias, 1991), in part due to feedbacks from dry land surface and a stronger cap inversion due to westerly advection from the Rockies or the Mexican plateau (Myoung and Nielsen-Gammon 2010). In addition, it suppresses the warm humid air transported by southerly winds from Gulf of Mexico in the lower troposphere that produce a large-scale environment conducive to rainfall in all seasons. Thus, an adequate representation of the middle tropospheric ridge, low-tropospheric zonal and meridional wind, and the circulation change associated with ENSO is central for demonstrating the credibility of the models for simulating droughts over SC US.

Although drought has occurred frequently in recent years, mean annual rainfall over the SC US has been increasing over the last century (e.g., Dai et al. 2004; Trenberth et al. 2007). This increase of rainfall appears to be correlated with the global scale SST warming (Wang et al. 2010, their Figs. 6c, 6d and 7b). By contrast, CMIP3 climate models have collectively projected a decrease of winter and spring rainfall by 5% to 30% by the late 21st century (Karl et al. 2009, Jiang and Yang 2012). CMIP5 climate models (Taylor et al., 2012) have included more comprehensive representations of many climatic processes with finer spatial resolution and more ensemble members for the simulations of each model and scenario compared to those for the CMIP3 models. How realistically do they represent current climate? What model qualities affect climate projections for the SC US? We investigate these questions with the ultimate aim of informing regional decision makers for future regional water resource planning.

Whether model quality would have a significant impact on climate projections has been debated. For example, Pierce et al. (2009) show that an ensemble mean, especially a multi-model ensemble mean projection, can out-perform even the best quality model.

However, over some regions, models may share a similar bias and if so it remains unclear whether multi-model ensemble averaging can effectively reduce such a bias. In addition, a demonstration of model quality, in many cases, is a prerequisite by policy makers for incorporating climate projection into their decision-making processes. This work aims to explore additional ways for reducing uncertainty in climate projections for the regions where most of climate models share similar biases, a condition different from those evaluated in Pierce et al. (2009).

Past studies have focused on assessment of climatology, natural variability and trends. These are important measures of the model credibility. For regional climate projections, additional metrics, especially related to links between regional climate change and anthropogenic global climate change are needed. For example, an evaluation of trends for the period of a few decades with a few climate model simulations can be strongly influenced by random internal variability (Deser et al. 2012), i.e., an agreement between a modeled and observed variable can be a random coincidence, rather than a demonstration of the capability of a model for prediction.

One way to address this issue is to examine the relationship between regional climate change and the global warming trend, rather than a regional climate trend alone. Such a relationship can be evaluated by observations. This study uses such a relationship as a key metric in assessing the quality of climate models, along with other metrics of large-scale circulation variables and their relationships with ENSO, AMO and global SST warming pattern, to evaluate the credibility of the climate models.

2.2: Datasets, Models and Methodologies

2.2.1: Datasets:

We used the Climate Prediction Center (CPC) US-Mexico daily gridded rainfall dataset (Higgins et al., 1996) for continental US between 22.5°N-40°N and 110°W-90°W. We combine its archival (from 1948-2004 at 1° resolution) and real-time (2001 to present at 0.25° resolution) components to obtain a continuous time series from 1950-2005. These data are re-mapped to a 2.5° resolution to match the lowest resolution of the CMIP5 models. Daily Tmin and Tmax were obtained from the Global Historical Climatology Network (GHCN) dataset (Vose et al., 1993), and gridded to 2.5° resolution using the Weaver Analysis technique. In the absence of adequate long-term measurements of ET, we use the monthly ET provided by the North American Land Data Assimilation (NLDAS) of the Goddard Land Data Assimilation Data System (GLDAS) (Rodell et al., 2004) obtained from http://mirador.gsfc.nasa.gov. The monthly Sea Surface Temperature (SST) data are obtained from the Extended Reconstructed SST

dataset (ERSSTv3b, Smith et al., 2008) for the period 1901-2005. The fields of 500 hPa geopotential height (Z500), and zonal and meridional winds at 850 hPa (U850, V850) are obtained from the National Center for Environmental Prediction (NCEP) reanalysis (Kalnay et al., 1996; Kistler et al., 2001)

2.2.2: CMIP5 models and the simulations used in this study

CMIP5 (http://cmip-pcmdi.llnl.gov/cmip5/) was organized by the World Climate Research Programme (WCRP). CMIP5 model outputs are archived by the Program for Climate Model Diagnosis and Intercomparison (PCMDI). Over 20 modeling groups from all over the world have participated in this project and conducted a variety of designed experiments (Taylor et al., 2012). We selected the following models as described in Table 1. Except for GFDL-ESM2M and GFDL-ESM2G, each model has more than three ensemble members for a specific experiment or scenario. We use ensemble averages for each model to improve the signal-to-noise ratio of the modeled fields and to give an equal weight to each model in the multi-model ensemble mean, except for analyses of the probability distribution function (PDF) of Tmax, Tmin, and rainrate, which are performed using a randomly selected single simulation. GFDL-ESM2M and GFDL-ESM2G each only provide one simulation per experiment. Their results can be strongly influenced by random noise (e.g., Deser et al. 2012). The historical simulations are driven by all the natural and anthropogenic forcings and are mostly from 1850 to 2005. We used the time period of 1950-2005 for model evaluation when observations are of adequate quality, and the period of 1979-2005 as the reference to compare with the projected climate for the period of 2073-2099 derived using the Representative Concentration Pathways (RCPs, Meehl and Hibbard, 2007a; Hibbard et al, 2007; Moss et al, 2010) scenarios of RCP4.5 and RCP8.5 that assume that the global mean radiative forcing will be stabilized at 4.5 Wm^{-2} and 8.5 Wm^{-2}, respectively, after 2100.

Table 2.1: Description of CMIP5 models used in this study

Model (Fig marker)	Institute (Country)	Available Ensembles	Components (Resolutions)	Calendar	Reference
CCSM4 (A)	National Center for Atmospheric Research (USA)	6	F09_g16 (0.9×1.25_gx1v6)	No leap	Gent et al., 2011
GFDL-ESM2M (B)	NOAA/Geophysical Fluid Dynamics Laboratory (USA)	1	Atm: AM2 (AM2p14, M45L24) Ocn: MOM4.1 (1.0° lat ×1.0° lon, enhanced tropical resolution: 1/3 on the equator)	No leap	John Dunne et al., 2012
GFDL-ESM2G (C)	NOAA/Geophysical Fluid Dynamics Laboratory (USA)	1	Atm: AM2 (AM2p14, M45L24) Ocn: MOM4.1 (1.0° lat ×1.0° lon, enhanced tropical resolution: 1/3 on the equator)	No leap	John Dunne et al., 2012
GISS-E2-R (D)	NASA/Goddard Institute for Space Studies (USA)	5	Atm: GISS-E2 (2.0° lat ×2.5° lon) Ocn: R	No leap	Schmidt et al., 2006
HadGEM2-CC (E)	Met Office Hadley Centre (UK)	3	Atm: HadGAM2 (N96L60) Ocn: HadGOM2 (Lat: 1.0-0.3 Lon: 1.0 L40)	360 d/y	Collins et al., 2011; Martin et al., 2011
MPI-ESM-LR (F)	Max Planck Institute for Meteorology (Germany)	3	Atm: ECHAM6 (T63L47) Ocn: MPIOM (GR15L40)	Gregorian	Raddatz et al., 2007; Marsland et al., 2003
IPSL-CM5A-LR (G)	Institut Pierre Simon Laplace (France)	5	Atm: LMDZ4 (96×95×39, 1.875° lat ×3.75° lon) Ocn: ORCA2 (2×2L31, 2.0° lat ×2.0° lon)	No leap	Marti et al., 2010
MIROC5 (H)	AORI, NIES & JAMSTEC (Japan)	4	Atm: AGCM6 (T85L40) Ocn: COCO (COCO4.5)	No leap	Watanabe et al., 2010
MRI-CGCM3 (I)	Meteorological Research Institute (Japan)	3	Atm: GSMUV (TL159L48) Ocn: COM3 (1×0.5L51)	Gregorian	Yukimoto et al., 2011

2.2.3: Metrics of model evaluation

Gleckler et al. (2008) and Pierce et al. (2009) have recommended metrics for a comprehensive evaluation of the general performance of global climate models. We select a subset of the climate variables from their recommended metrics, with additional variables that are highly relevant to the processes that control the development and occurrence of droughts.

In particular, previous studies have shown that a persistent high pressure system and middle tropospheric ridge, and dry land surface are key conditions for summer drought over the SC US (e.g., Hong and Kalney 2002, Myoung and Nielsen-Gammon 2010). Strong westerly winds advect dry and warm air from the Mexican Plateau and Rockies to the SC US and enhance cap-inversions in the lower troposphere. Weakened lower tropospheric southerly winds fail to bring warm and humid air from the Gulf of Mexico, creating an unfavorable condition for rainfall. Dry conditions during late spring sets the stage for summer droughts. Prolonged droughts from winter to summer often lead to extreme drought. These conditions also favor the occurrence of extreme summer surface temperature, because of strong inverse correlation between high surface temperature and dry land surface in this region (Madden and Williams 1978).

Drought over the SC US is initiated by La Niñas in boreal winter, and could be intensified by a positive phase of the Atlantic Multi-decadal Oscillation (AMO, McCabe et al. 2004; Hu and Feng, 2008, Mo et al. 2009, Kushnir et al. 2010, Nigam et al. 2011). However, ENSO and AMO are random modes of internal variability. Thus, we focus on the realism of ENSO teleconnection pattern and the relationship between regional rainfall anomalies and ENSO. A couple of centuries could be needed to adequately assess ENSO variability (Wittengberg 2009; Stevenson 2012). Thus, significance of our evaluation on how such natural climate variability influences the SC US climate is somewhat limited by lengths of climate records and historical simulations. The duration of the available observations is more inadequate for evaluation of AMO related change.

In addition, Wang et al. (2010) have suggested a statistical connection between an increase of summer rainfall over SC US and global increase of SSTs. Because this global increase of SST is attributable to anthropogenic forcing (e.g., Barnett et al. 2001), we will evaluate this relationship as an indicator of regional rainfall sensitivity to forced global climate change.

To investigate how models' uncertainties influence climate projections, we compare the multi-models ensemble projections with and without under-performing models.

2.2.4: Analysis methods

The SC US domain in our analysis includes Texas and portions of New Mexico, Oklahoma, Louisiana, Arkansas, Kansas and Missouri (Fig. 1). The domain was chosen based on the spatial pattern of the observed rainfall variability (Higgins et al. 1997) and trend over US for the period of 1958-2008 reported in the 2009 Report on Global Climate Change impact in the United State by US Global Climate Research Program (Karl et al. 2009). The domain is also chosen to be large enough to include enough grid points from the relative low spatial resolutions of the CMIP5 models.
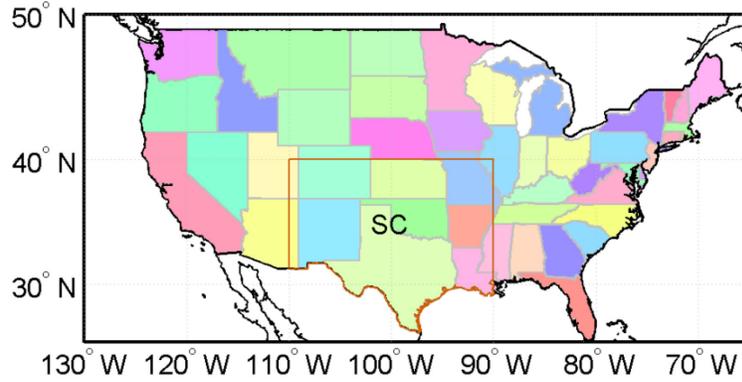
Fig. 2.1: Spatial domain of the SC US defined in this study

The root-mean square error (RMSE) is used as a concise way of comparing statistical characters of a modeled and observed field (Gleckler et al. 2008). We apply RMSE to determine how realistic the spatial patterns in the models are. The RMSE is calculated as follows:

$$RMSE = \sqrt{\frac{1}{N} \Sigma \left(\overline{M}_{x,y}^{t} - \overline{O}_{x,y}^{t} \right)^2} \qquad (1)$$

where M represents a modeled field and O represents a corresponding observed field. The indices x, y correspond to the spatial location, t is the time, and N is the total number of the spatial points.

Following Schubert et al. (2009), the global SST warming mode is represented by the leading mode of the Rotated EOF (REOF, Barnston and Livezey, 1987; Richman 1987; O'Lenic and Livezey, 1988), or REOF1, of the annual and summer (JJA) global sea surface temperature (SST) anomalies. The observed REOF1 as seen in Schubert et al. (2009) is mostly a trend in SSTs. It appears to consist of a global scale warming pattern and some regional details; the most pronounced is cooling in the North Atlantic and warming over the Indian Ocean. The time series of the REOF1 mode shows a monotonic rise in SSTAs over the century.

The Niño3.4 index is computed as the domain averaged SST anomalies over the region of 160°E-90°W and 5°N-5°S. Statistical significant tests of correlation coefficients are determined by the Student-T test.

2.3: Evaluation of Historical Simulations

2.3.1: Regional climatology and variability

a. Surface conditions

Figure 2 compares the seasonal cycles of surface air Tmax, Tmin and surface air specific humidity (q), P, ET and net water exchange between the atmosphere and surface (P-ET) simulated by the 9 CMIP5 models to those derived from the GHCN data, NOAA CPC US-Mexico daily gridded datasets and NCEP reanalysis. The models capture the seasonal variations of Tmax and Tmin over the SC US. However, they appear to consistently underestimate Tmax values by as much as 5-7 °C during winter, and spring and fall (Fig. 2a). In summer, Tmax values in one third of the models (HadGEM2-CC, CCSM4 and MIROC5) agree with observations, but they are underestimated in two-thirds of the models by as much as 5 °C. The multi-model ensemble mean shows a similar patterns and biases as those of individual models.

Tmin values in most of the models and multi-model ensemble mean agree well with those observed (Fig. 2b). MIROC, CCSM4 overestimate Tmin by 1-2 °C in summer and fall, whereas HadGEM2, IPSL over underestimate Tmin by 3 °C in winter. The modeled surface air q agrees well with the observations, except for HadGEM2-CC and IPSL (Fig. 2c).

Observations show that rainrate over the SC US is generally higher than 2 mm/day during April to October and below 1.5 mm/day from October to March (Fig. 2d). Peak rainfall occurs in May, about 2.5 mm/day, and annual minimum occurs in January, about 1.5 mm/day. The CCSM4 and MPI best capture this seasonal pattern. HadGEM2, GFDL-ESM2M and MRI show a spurious mid-summer dry period, leading to a semi-annual cycle peaking between spring and early fall. IPSL shows a short summer peak of rainfall with very dry spring and fall seasons. Except for IPSL, models consistently overestimate rainfall by 0.5 to 1 mm/day with large inter-model discrepancies during spring and summer seasons.

Figure 2e shows that models generally capture the seasonal cycle of ET shown by NLDAS, although two-thirds of them underestimate the values of ET. The GISS model overestimates ET by as much as 250%, whereas IPSL and CCSM4 underestimate ET by nearly 30% in summer. The high bias of the multi-model ensemble mean is largely due to that of the GISS model.

P- ET represents the net water flux available to the surface, thus it has strong influence on meteorological drought, soil moisture and floods. Figure 2f shows that the P-ET estimated by observations and NLDAS is positive during fall, winter and spring (September to March) and peaks in winter at the rate of about 1 mm/day, and negative during summer (June-August) at about -1 mm/day. Most of the models capture this seasonal pattern of P-ET, but underestimate the magnitude of surface water loss (negative P-ET). The GISS-ER2 model substantially overestimates the magnitude of surface water loss due to its strong overestimate of ET (Fig. 3b), whereas CCSM4 does not capture the observed negative P-ET in summer. The multi-model ensemble mean shows good agreement with that observed due to a balance between overestimated and underestimated P-ET values among different models.
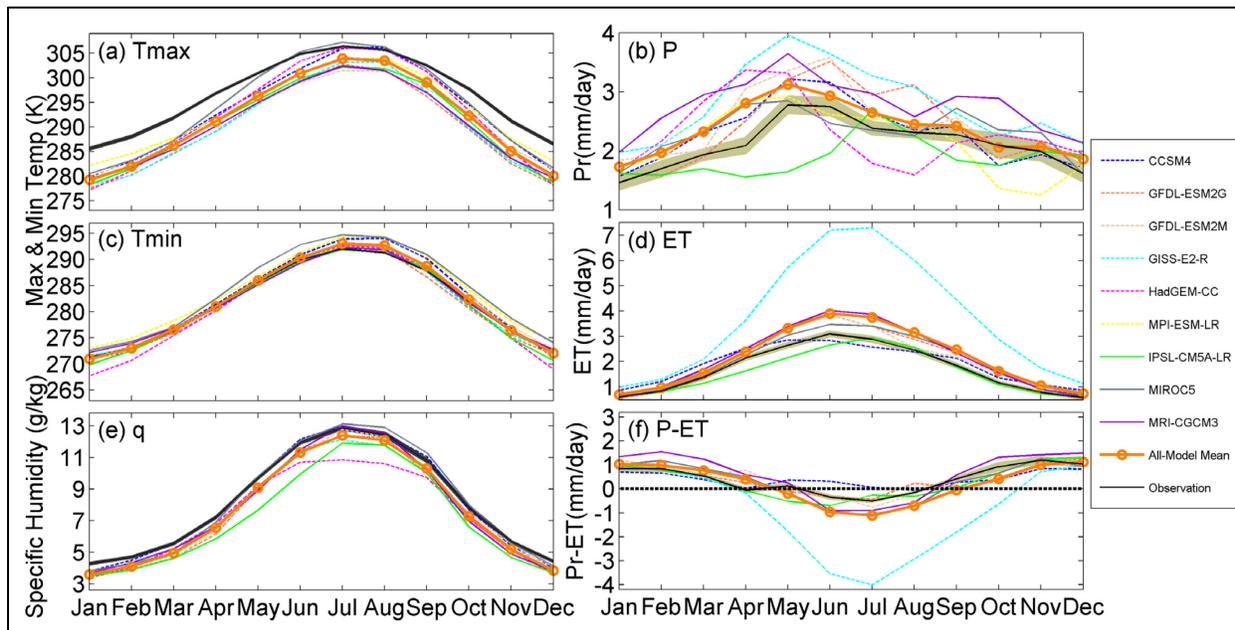
Fig. 2.2: Seasonal cycles of daily maximum and minimum surface temperature (Tmax, Tmin) and specific humidity (q), precipitation (P), evapotranspiration (ET) and the net downward water flux (P-ET) derived from observations and historical simulations of the CMIP5 models for the period of 1950-2005.

The PDFs of Tmax, Tmin, rainrate and P-ET are important in determining statistical distributions of extreme climatic events. Fig. 3a shows that Tmax has a distribution over the SC US that ranges between 23 °C − 33°C or about 72 °F − 90 °F skewed toward warmer Tmax values. The models capture the general shape of the PDF. However, they consistently underestimate the probability of hot to extreme Tmax (>33°C , or >90 °F), and overestimate probability of colder Tmax (< 12°C, or < 55 °F), except for MIROC5. The majority of the models and multi-model ensemble mean also capture the general pattern of PDF of Tmin (Fig. 3b) although they consistently underestimate probability of cooler Tmin < -3°C or < 27 °F). MIROC5 and CCSM4 also substantially overestimate the probability of warmer Tmin (17 °C − 27 °C or 63 °F − 81 °F).

Fig. 3c shows that the models consistently underestimate of probability of non-rainy days and extreme violent rainy events (>50 mm/day), and overestimate moderate rainy events (2.5-10 mm/day). These biases contribute to the overestimate of climatological rainfall (Fig. 2). HadGEM2-CC and MPI provide the most realistic PDF of rainrate. Except for IPSL and GFDL-ESM2M and GFDL-ESM2G, most of the models are skewed toward overestimating the weak positive P-ET values and underestimating the weak negative P-ET values (Fig. 3d). This is also constant with the wet biases shown in Fig. 2. CCSM4 and GISS-E2-R have the strongest biases in the PDF of the P-ET.
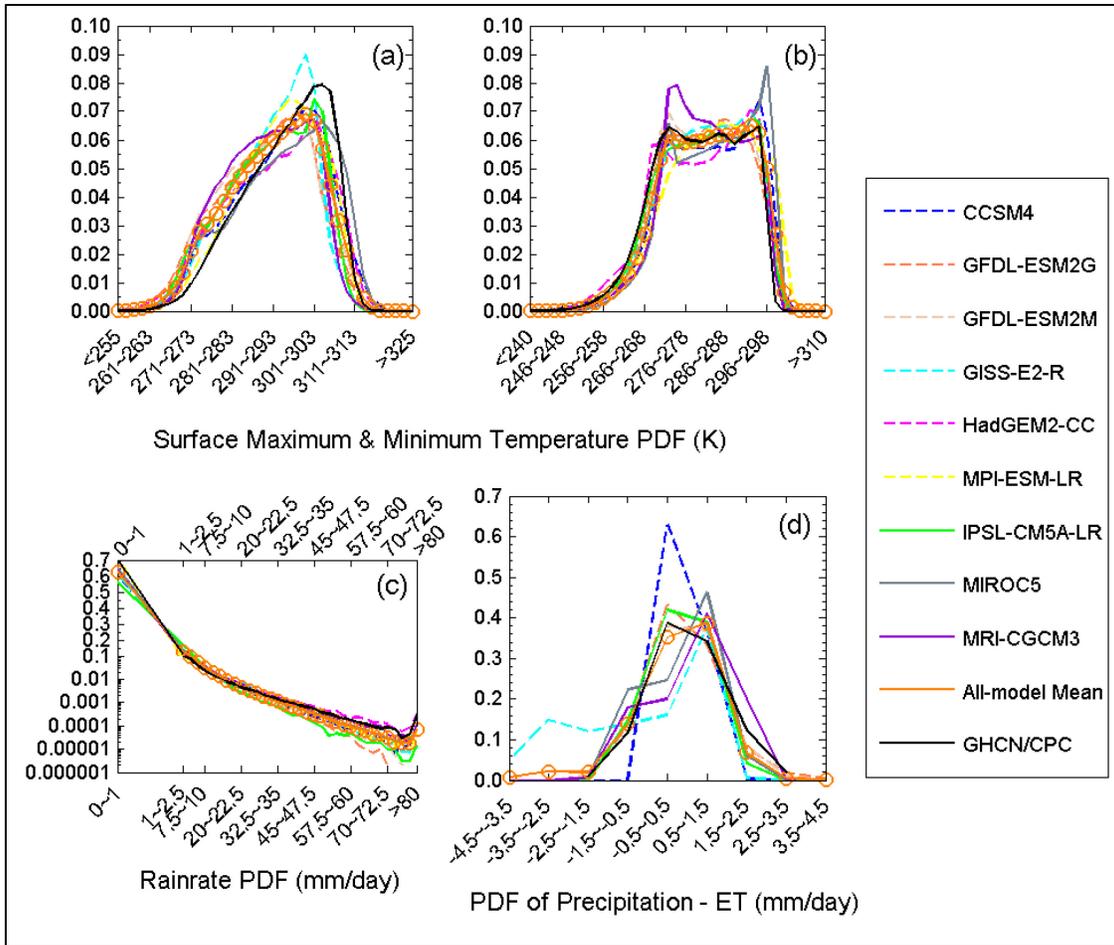
Fig. 2.3: Observed and modeled PDF of a) Tmax, b) Tmin, c) P, and d) P-ET for the period of 1950-2005. One ensemble member from each model is used.

b. Atmospheric circulation

To investigate the underlying causes of the biases in regional surface climate conditions, this section evaluates modeled atmospheric circulation patterns. Figure 4 summarizes the evaluation of modeled spatial patterns for Z500 (Figs 4a-4d), U850 (Figs. 4e-4h) and V850 (Figs. 4i-4l), respectively, for four different seasons. Figures 4a-4d show that all the models have nearly perfect spatial correlation with observations and the same standard deviations as those observed. The RMSEs are near zero except for the summer season (JJA). Thus, these models well capture the patterns of Z500 in winter and spring and fall seasons. In summer, the two GFDL models (B and C) best capture the Z500 spatial pattern, followed by CCSM4 and MIROC5. Other models show considerable errors in capturing the observed summer Z500 pattern, mainly due to their underestimate of the middle tropospheric ridge over the SC US (not shown). The latter is a key circulation feature associated with drought over SC US, and its underestimation would contribute to an overestimate of rainfall and underestimate of surface temperature in summer (Fig. 2). Figs. 4e-4h suggest that the modeled spatial patterns of U850 are generally well correlated with that observed (>0.9), although some models underestimate the variability (standard deviation) of the U850, especially in spring. Lower-level zonal wind advects dry and warm air from Mexican Plateau and Rockies, contributes to the occurrence and strength of the inversion in the lower troposphere, as is critical for initiating spring and summer drought (Hong and Kalney 2002, Myoung and Nielsen-Gammon 2010, Fernando et al. 2013). Thus, an underestimate of variability of the U850 could contribute to an underestimate of the occurrence of strong and extreme negative P-ET (Fig. 2f). Figs. 4i-4l show that the spatial patterns of V850 are somewhat less correlated with those observed and the spatial variability is underestimated (normalized standard deviation below 1). These discrepancies between modeled and observed V850 are especially apparent during the fall season (SON). Errors in V850 of models would in turn influence their transport of warm moist air from the Gulf of Mexico to the SC US.
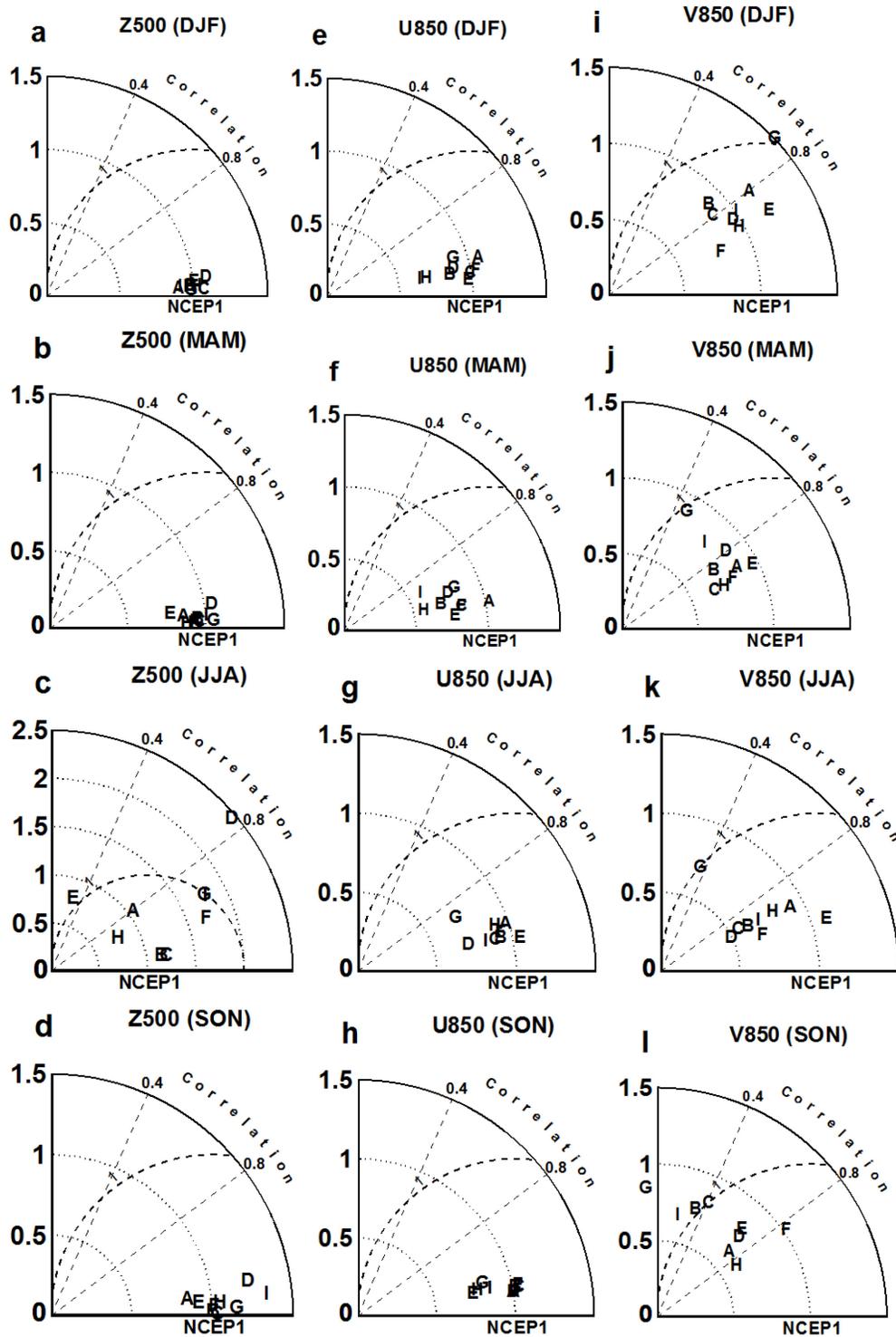
Fig. 2.4: Taylor diagram for spatial pattern of Z500, U850 and V850 in the four seasons in SC-US. The solid radial axis represents a normalized standard deviation of a modeled field by the corresponding observed field. The dash circular line presents the RMSE of 1 unit of the corresponding variable. The letter characters represent: A: CCSM4, B: GFDL-ESM2M, C: GFDL-ESM2G, D: GISS-E2R, E: HadGEM2-CC, F: MPI-ESM, G: IPSL, H: MIROC5, I: MRI-CGCM3.

2.3.2: Relationship with interannual and decadal climate variability modes

Whether or not climate models can adequately represent the connections between regional climate anomalies and their oceanic forcing is central in determining the frequency and intensity of droughts and probability of extreme temperatures and rainfall. We compare the modeled and observed correlation coefficients for the areal averaged rainfall anomalies over the SC US with the Niño index (Niño34) in Table 2. Observed rainfall over the SC US is significantly positively (negatively) correlated with El Niño (La Niña) only in winter (DJF). This seasonal dependence of correlation is only captured by the GISS-E2R. GFDL-ESM2M, GFDL-ESM2G, MIROC5, IPSL capture this relationship in winter, but also exaggerate its seasonal persistence during other seasons. CCSM4 and HadGEM2-CC show spurious correlation between the SC US rainfall and ENSO in spring, summer and/or fall, whereas MRI-CGCM3 does not show any relationship between the SC US rainfall anomalies and ENSO.

Table 2.2: Correlation between Niño3.4 and the SC US rainfall. Only values significant at 95% confidence level using the Student t-test are shown. Left side for each season is correlation with Nino3 and right side is with Nino4.

	DJF	MAM	JJA	SON
Obs	0.60			
CCSM4		0.77	0.55	0.62
GFDL-ESM2M	0.49	0.71		0.66
GFDL-ESM2G	0.57	0.52		
GISS-E2R	0.42			
HadGEM2-CC				0.41
MPI-ESM				
IPSL	0.44	0.53	0.53	
MIROC5	0.75			0.60
MRI-CGCM3				

The influence of ENSO on the SC US rainfall anomalies is determined by the ENSO teleconnection pattern. Fig. 5 shows the spatial pattern of the correlation between the Z500 anomalies and Niño34 index during winter (DJF) when regional rainfall anomalies are significantly correlated with ENSO indices for the period of 1950-2005. CCSM4 and GFDL-ESM2M best capture this tele-connection pattern. MIROC5 and GISS-E2-R are also qualitatively realistic. Other models cannot adequately capture this ENSO related tele-connection pattern.

The standard deviations of the Niño34 index normalized by those derived from observation are close to one in CCSM4, GFDL-ESE2M, GFDL-ESM2G, HadGEM2 and MIROC5. Thus, the magnitude of the Niño34 variability is comparable to those observed in these models. The variability of Niño34 index in GISS-E2-R, IPSL, MPI and MRI are only about 40% of that observed.
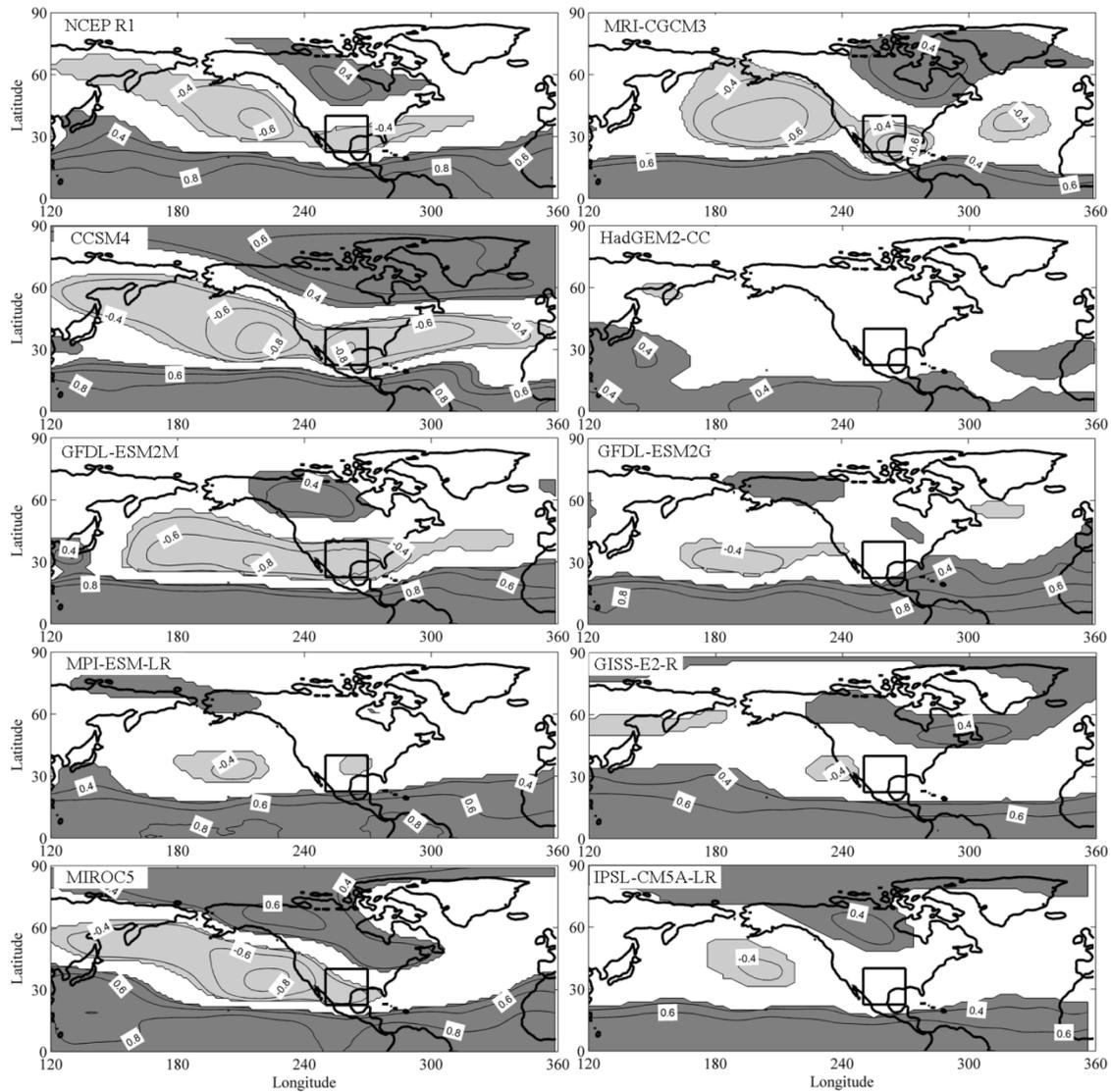
Fig. 2.5: Correlation pattern between Z500hPa anomalies and Niño34 index obtained from the NCEP reanalysis and the historical simulations by the nine CMIP5 models for the period of 1950-2005.

2.3.3: Relationship with global SST warming mode

How well can CMIP5 models represent the patterns of the SC US as part of the increase of global surface temperature? To explore this question, we first evaluate the spatial pattern of the REOF mode of SST anomalies that represents the global increase of SST for JJA, the season when the increase of rainfall over SC US is most evident (e.g., Wang et al. 2009) and the influences of ENSO and PDO are relatively low (e.g., Grassi et al. 2012). This mode is not correlated with either ENSO or PDO variation. As the leading REOF mode of the observed SST anomalies (Schubert et al. 2009), it shows warming over most of the global ocean, except for over high-latitude North Atlantic and northwestern Pacific, and equatorial eastern pacific (Fig. 6). The spatial pattern of this global SST warming mode is best captured by GFDL-ESM2G and GISS-ER2 as their leading REOF mode. CCSM4 and MPI also capture the general pattern of the warming mode, although they either overestimate the cooling over the North Pacific or over the equatorial Pacific. They also closely capture the trend of the principle component of the REOF1 (PC1) of the observed SST, whereas other models, including the GFDL-ESM2G and GISS-ER2, underestimate this observed trend. In HadGEM2-CC, MIROC5 and GFDL-ESM2M models, ENSO emerges as the leading REOF mode of SST anomalies. The global SST warming mode emerges as the second or even the third leading REOF mode, suggesting these models underestimate the influence of the global SST warming or over-estimate the influence of ENSO on SST variation.

In Fig. 7, we compared the modeled correlation coefficients between the changes of summer rainfall over the SC US and the global SST warming mode to that observed for summer season (JJA). Most of the models cannot adequately reproduce this observed relationship. For these models that capture the global SST warming mode as the leading REOF mode, one with more realistic spatial pattern of this mode (high spatial correlation) appears to show a more realistic correlation between this global warming SST mode and change of the rainfall over the SC US in summer. This relationship may suggest that errors in the warming spatial pattern may in part contribute to the error of its relationship with the change of summer rainfall in the SC US. Such a relationship does not exist for the models that show the global SST warming mode as the second or third mode.

We note that Wang et al. (2009) have attributed the increase of rainfall over the central US to the PDO through a suite of climate model experiments for the period of 1950-2000. Their global SST warming mode that resembles the pattern in Fig. 6 forces a drying, rather than wetting, over the SC US in all seasons in the National Aeronautics and Space Administration (NASA) Seasonal-to-Interannual Prediction Project (NSIPP)-1 model. Whether this discrepancy is due to the model's limitation in representing impact of global warming SST on US rainfall anomalies, or whether the observed regression pattern mis-represents the relationship between global warming SST mode and US rainfall anomalies need to be further investigated.
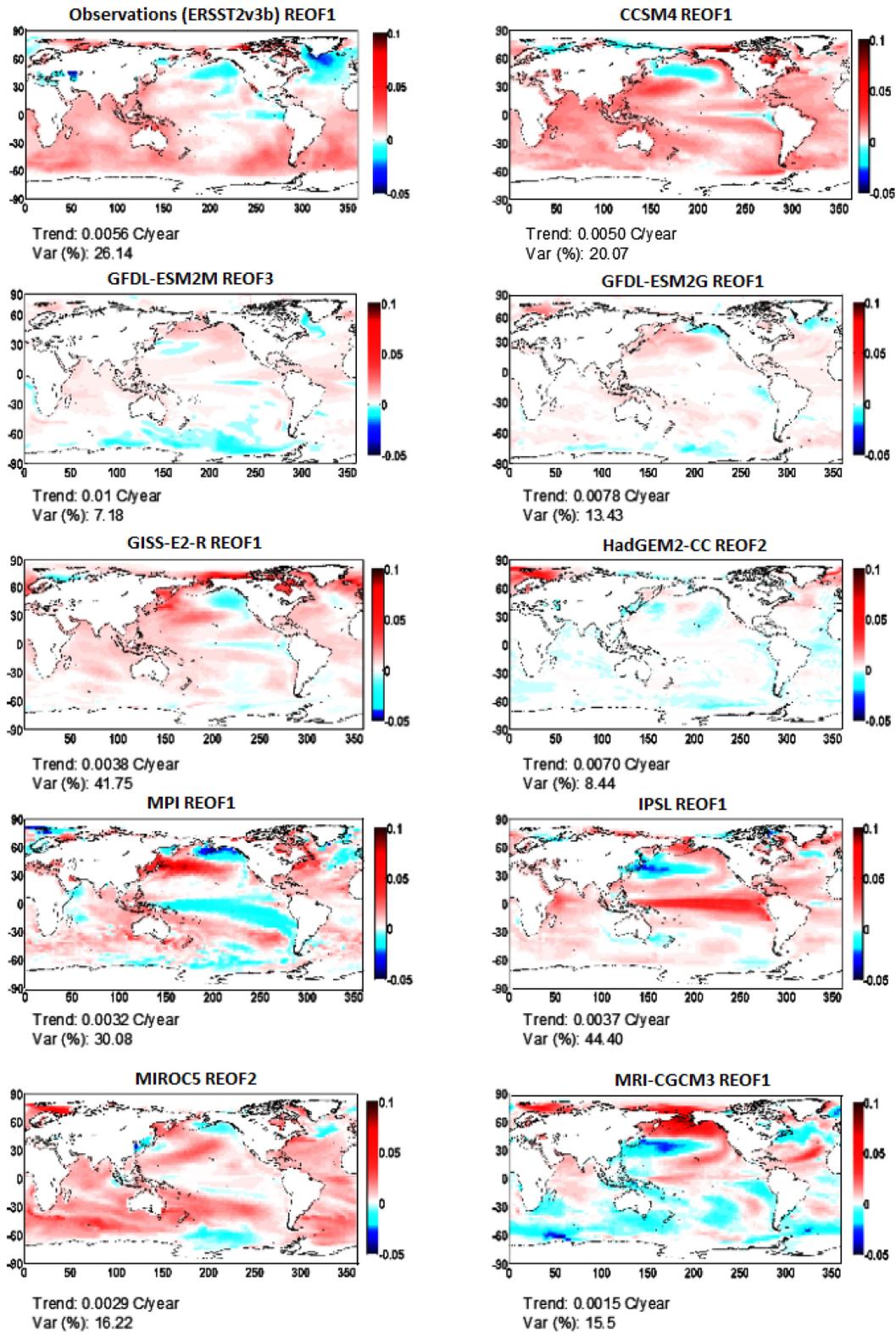
Fig. 2.6: The leading mode warming REOF (REOF1 in observations) derived from observed and modeled SSTA from the nine CMIP5 models.
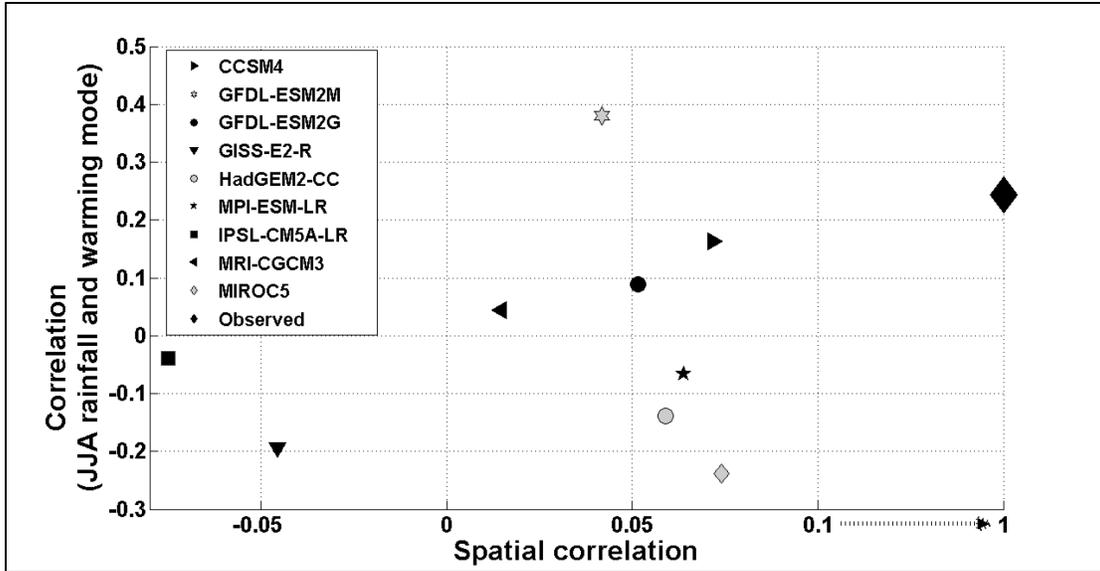
Fig. 2.7: Correlation coefficients between the SC US summer rainfall anomalies and the principle component (PC) of the global SST warming mode and the spatial correlation between the observed and modeled SST warming mode for the nine CMIP5 models and observations. The dark black symbols represent the models in which leading REOFs represent the global SST warming mode. The grey symbols represent the models in which the leading REOFs do not represent the global SST warming mode. Observed correlation coefficient is indicated by big black diamond symbol.

2.3.4: Discussion of model performance

For assessing overall performance and its implications for the models in projecting climate change over the SC US, we broadly bin the models into three performance categories based on the results shown in Sections 3.1-3.3. Models that realistically capture the patterns of the spatial or temporal variability, changes and correlation for a selected climate variable are marked as the top performing (Class-T) models for that variable. The models that partially agree with the observations, including the signs of correlation or changes, are ranked as average performing (Class-A) models. Models that show no resemblance to observations, e.g., showing wrong signs of correlation between regional climate responses to external forcings, are marked as the under-performing (Class-U) models.

Following the above guidelines, the models' performance in representing the SC US regional climate is summarized in Table 3. Overall, the HadGEM2-CC, IPSL, MRI-CGCM3 under-perform for 40% or more of the metrics we evaluated and produce unrealistic seasonal cycles of precipitation. GISS-ER2 too strongly overestimates ET, leading to a large bias in P-ET. Because these "U" models have larger uncertainties not only in representing the regional climate condition and water balance, but also the processes that control the variability and change of the regional climate, they are less credible in their climate projections for the SC US region. Thus, we will evaluate multi-model ensemble projections with and without these models to assess how these "U" models influence the ensemble climate projection.

Table 2.3: Summary of the models performance for the SC US regional climate

Variables	Models								
	CCSM4	GFDL-ESM2G	GFDL-ESM2M	GISS-E2-R	HadGEM2	MPI	IPSL	MIROC5	MRI
	Correlation with global SST warming:								
a_{GW}	T	U	T	U	U	U	U	U	A
GW_{SST}	A	T	U	T	U	A	A	U	A
	Seasonal cycle:								
Tmax	T	A	A	A	T	A	U	T	A
Tmin	A	T	T	T	U	T	U	A	T
q	T	T	A	T	U	T	U	T	T
P	T	U	U	A	U	T	A	A	U
ET	U	A	A	U	A	A	A	A	A
	Probability Distribution								
PDF_{Tmax}	U	U	U	U	U	U	U	U	U
PDF_{RR}	A	A	A	A	A	A	A	A	T
PDF_{P-ET}	U	T	T	U	U	U	A	U	U
Z500	A	U	U	U	A	A	U	A	U
U850	T	A	A	A	A	T	T	A	A
V850	A	A	A	A	T	A	A	A	A
	Natural variability								
$r_{p,Niño34}$	U	A	A	T	U	U	U	A	U
$S_{Z500, Niño34}$	A	A	A	U	U	U	U	U	U

T: Generally realistic pattern, A: partially realistic, Ranking U: No resemblance to those observed
a_{GW}: Linear regression coefficient between the SC US summer rainfall anomalies and the PC of the global SST warming mode of the REOF analysis of global SST anomalies for the period of 1950-2005; GW_{SST}: Spatial pattern of the global SST warming mode; PDF_{Tmax}, PDF_{RR} and PDF_{P-ET}: Probability distribution of daily maximum surface temperature, rainrate, and P-ET, respectively; $r_{p,Niño34}$: Correlation coefficient between the SC US rainfall anomalies and Niño34 index; $S_{Z500, Niño34}$: Spatial patterns of the regression between Z500 anomalies and Niño34 index.

2.4: Climate Projections for the Late 21st Century

To assess climate change over the SC US in the future, we evaluate projected regional climate conditions for the period of 2073-2099 (referred to as the late 21st century) under the RCP4.5 and RCP8.5 scenarios, respectively, and compare them to the historical simulations for the period of 1979-2005 (referred to as the recent past) for each model. Because several models only provide one simulation for each future scenarios, we randomly select one realization for each model in assessing the projected changes of the PDF of Tmax, Tmin, P and P-ET in future for the RCP4.5 and RCP8.5 scenario, respectively (Figs. 8-11). Ensemble means of individual simulations for each model and each scenario are used for assessing the changes of seasonal cycles of the P, ET and P-ET in Fig. 12. The projections of multi-model ensemble means of all the nine models and those without the "U" models will be compared in our discussion. Because of the model biases as shown in Section 3, we will focus more on changes of the climate conditions than on absolute values. For brevity we do not show the analysis of projected circulation change.

2.4.1: Projected changes in surface climate conditions

Fig. 8 shows the projected Tmax distributions based on a single simulation of each model over the SC US by the late 21st century compared to that in the recent past. Under the RCP4.5 scenario, the individual models and the multi-model ensemble mean consistently project a more skewed PDF toward warm temperatures, except for MIROC5. The occurrence of warm temperatures that range from 301K (28˚C or 82.4˚F) to 316K (43˚C or 109.4˚F) increases 25% to 50% relative to those of the recent past. The occurrence of Tmax cooler than 3˚C decreases. The occurrence of Tmax with medium values of 275K-283K (2˚-10˚C) decreases slightly. The ensemble projection without "U" models projects a stronger increase of Tmax warmer than 313K (40˚C or 104˚F) than that including all nine models.

Under the RCP8.5, the projected change of PDF patterns are similar to those of RCP4.5 scenario, but warmer Tmax, ranging from 301K-316K (28˚C to 43˚C), will increase by 50%-100% relative to their occurrence in the recent past. Although the peak of Tmax distribution will be the same as projected by the majority of the models, more models (HadGEM2, MPI, MIROC5) project a shift of the peak Tmax distribution to 305K-315K (32˚C-42˚C, not shown). Such projections suggest that the summer extreme temperatures during the late 20th century will become normal in future. Again, the projected changes of Tmax distribution by the ensemble mean without "U" models shows a similar increase of the extreme warm Tmax (>305K or >32˚ C) of that by all the nine models.

The projected changes of Tmin distribution is shown in Fig. 9. For both emission scenarios, the models consistently project more occurrences of Tmin that exceed 298K (25˚C) and a decrease of Tmin below 273K (0˚C) in future. The occurrence of medium Tmin will not change by more than a few percentages. Under the RCP8.5 scenario, the increase of the occurrence of Tmin warmer than 298K (25˚C or 77˚F) to 303K (30˚C or 86˚F) will be double of that under the RCP4.5 scenario. The ensemble projections with and without the "U" models are very similar.

Fig. 10 shows projected changes of distribution of rainfall intensity in the late 21st century. The majority of the models and multi-model ensemble mean suggest an increase of non-rainy and light rainy days, and a decrease of light to moderate rainy days (1-10 mm/day) for both emission scenarios. The magnitude of these changes is nearly doubled under the RCP8.5 scenario than under the RCP4.5 scenario. The ensemble mean projections with and without the "U" models show the similar pattern of PDF changes, although that without "U" models shows a weaker decrease of light to moderate rainy days relative to that by all the models.

Projected future changes of the PDF of the net surface water flux (P-ET) are shown in Figure 11. Under the RCP4.5 scenario, there is large inter-model discrepancy in term of sign of the changes.

Consequently, the ensemble projections show little change. These results suggest that the projected changes are probably dominated by random natural variability and forced changes are not robust. Under the RCP8.5 scenario, a majority of the models, thus the multi-model ensemble means, project an increase of weak negative P-ET and decrease of weak positive P-ET. MIROC5, GISS and MRI –CGCM3 project much stronger changes, whereas CCSM4 project much weaker changes, compared to the multi-model ensemble mean projections. Removal of the "U" models does not significantly change the multi-model ensemble projections.

The seasonal cycle of the P-ET is crucial for water resource management. We evaluate its future change in Fig. 12. The projected changes are noisy with large inter-model discrepancies under both emission scenarios. Under both the RCP4.5 and RCP 8.5 scenarios, there are very large inter-model discrepancies in both P and ET, even in term of sign of the changes. However, the "U" models (HadGEM-CC, MRI-CGCM3, IPSL, GISS-E2R) are outliners in these projections. The multi-model ensemble mean shows a weak increase of P in spring and fall, but decrease during summer. The changes of ET generally follow that of P, except for increase in winter. Because the projected changes of ET general exceed those of P, P-ET decreases in winter, spring and fall, and generally unchanged in summer. Under RCP4.5, ensemble projections without the "U" models show stronger decreases of ET and thus less P-ET deficits in late spring and summer (May-October), whereas under the RCP8.5 scenario, the ensemble projections without the "U" models show stronger decreases of winter and spring P, hence P-ET than the ensemble projections with nine models.

The projected increases of surface water loss during winter, spring, and fall, especially by the models that appear to better capture the processes that control rainfall variability and change, imply a strong increase of dry spells. These changes can contribute to disproportionally large increase of warm and hot Tmax as shown in Fig. 8.

Daily Maximum Surface Temperature Probability Distribution Function (K)
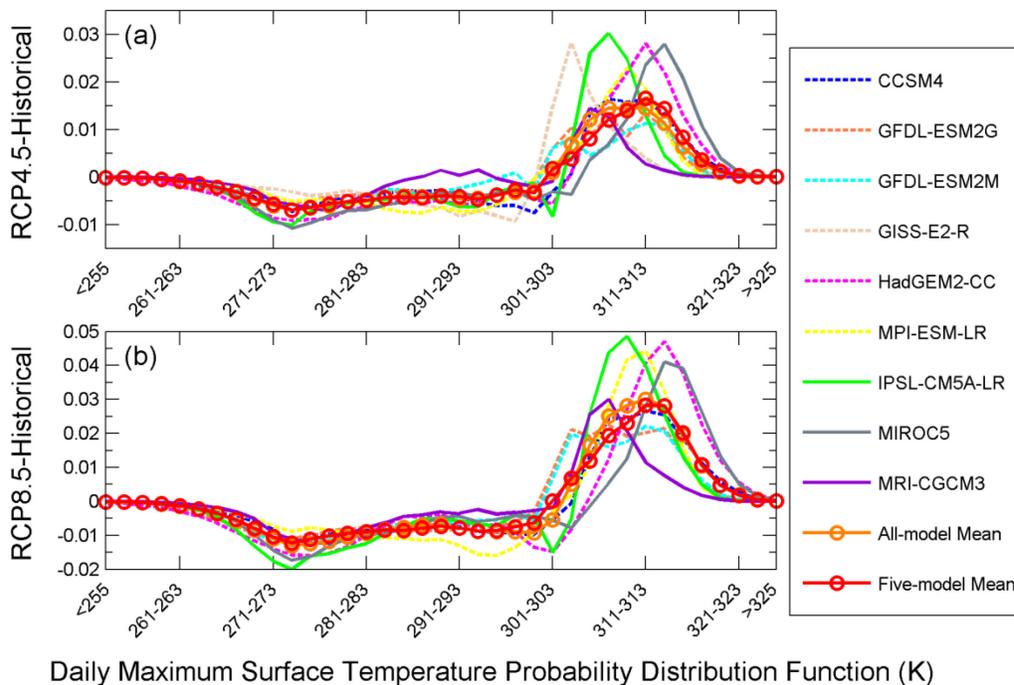
Fig. 2.8: Projected Tmax during period of 2073-2099 under the RCP4.5 and RCP8.5 scenarios, compared to that from the historical simulations of the CMIP5 models during the period of 1979-2005.
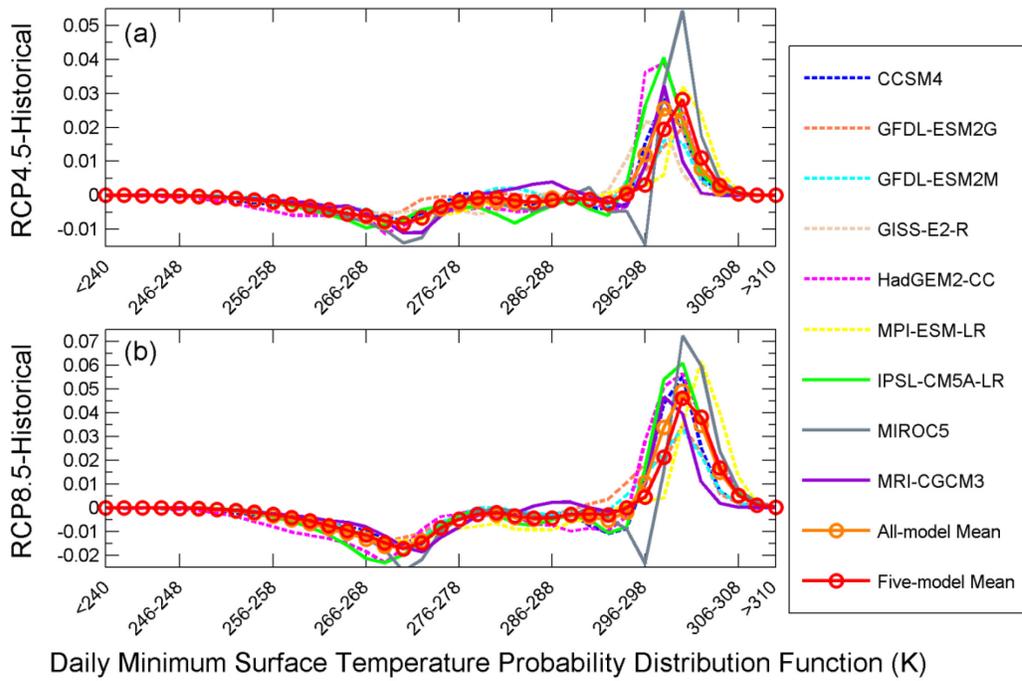
Fig. 2.9: As in Fig. 8 but for Tmin.
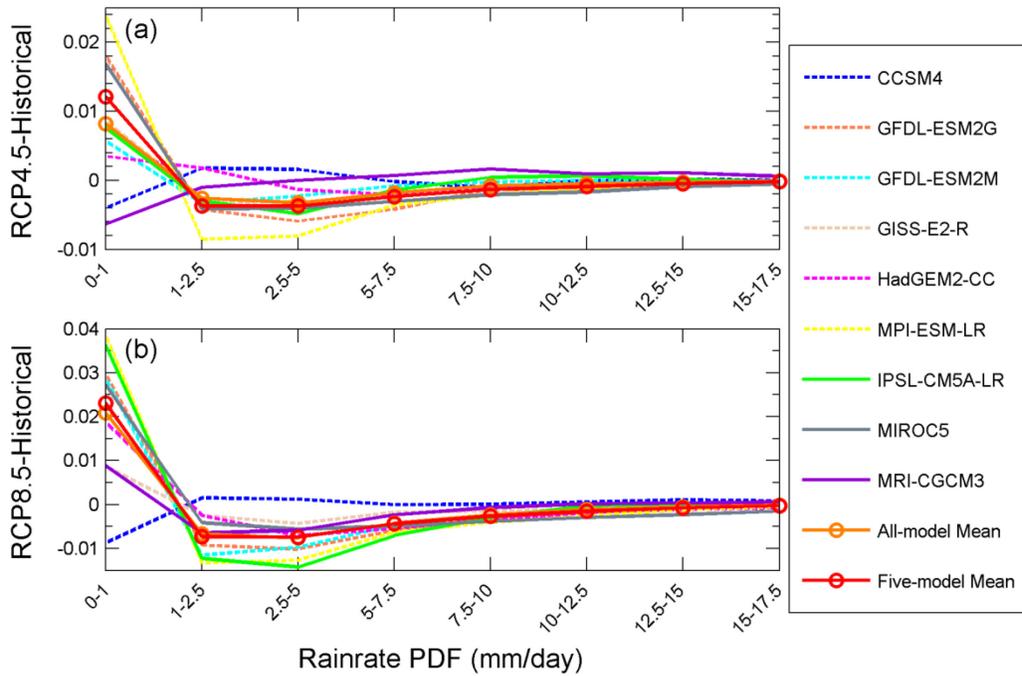
Fig. 2.10: As in Fig. 8 but for the projected changes of the PDF of P for the RCP4.5 and RCP8.5 scenario, respectively. The units are mm/day.
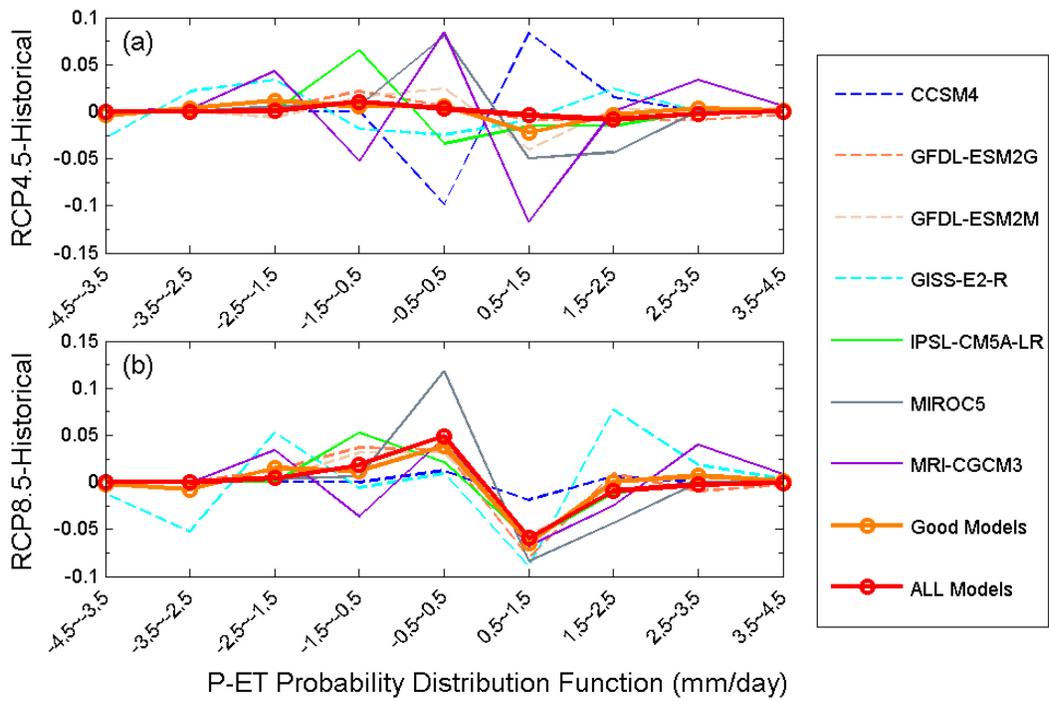
Fig. 2.11: As in Fig. 8 but for the PDF of P-ET.
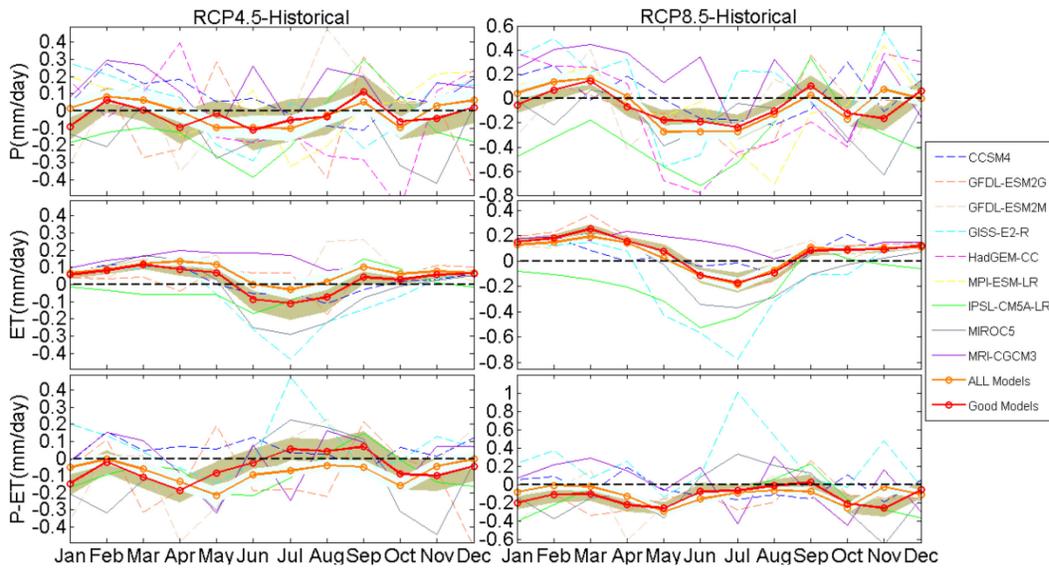
Fig. 2.12: Changes of climatological seasonal cycles of P, ET and P-ET between the period of 2073-2099 for the RCP4.5 and RCP8.5 scenarios and those from the historical simulations for the period of 1979-2005.

2.5: Conclusions and Discussion

We have evaluated the performance of nine CMIP5 models in representing the SC US regional surface climate, its variability and changes, the key large-scale circulation patterns, and their links to ENSO and the global scale SST warming mode, as a basis to assessing the fidelity of these models for climate projections over this region. A novel aspect of this evaluation is its focus on the key processes that control the droughts and their relationships with global scale climate variability and change.

The evaluation suggests that the models generally adequately reproduce the observed patterns of the seasonal cycles and the probability distributions of the surface temperature, humidity and rainfall. However, the majority underestimates Tmax and q and overestimate Tmin and P, especially during spring and early summer. The excessive rainfall is due to an underestimate of non-rainy and light rainy days (<1 mm/day) and an overestimate of moderately rainy days (1-10 mm/day). These models also consistently underestimate the occurrence of days with heavy to violent rainfall events (>10 mm/day).

The models very well capture the spatial pattern of the Z500 in all seasons except for summer. During summer, about a half of the models underestimated the mid-tropospheric ridge, which could contribute to overestimate P and underestimate Tmax in summer. The spatial pattern of the U850 is also well represented by the models in all seasons, except for spring. The errors of U850, especially the underestimate of westerly U850 in spring could lead to underestimation of the lower-troposphere static stability, hence contributing to the wet and cold biases in spring. The spatial patterns of V850 are also generally well simulated, except for during fall season. Most of the models appear to underestimate the spatial variability of the V850. These errors could influence moisture transport from the Gulf of Mexico to the SC US.

Only a few models (CCSM4, GFDL-ESM2G and GFDL-ESM2M) partially capture the teleconnection pattern associated with Niño3.4 index. However, these models tend to overestimate persistence of the ENSO influence on the SC US rainfall anomalies, and are unable to capture the seasonality of such influences. The GISS-E2R is the only model that adequately captures the seasonal dependence of the relationship between the SC US rainfall anomalies and ENSO. In addition to uncertainty of the models' physics, the apparent poor performance of the ENSO teleconnection patterns could be in part due to insufficient sampling of ENSO within our short analysis period (Wittengberg 2009; Stevenson et al. 2012). Nevertheless, these uncertainties highlight the challenge of modeling the impact of ENSO on regional rainfall in global climate models.

Several models (CCSM4, GFDL-ESM2G, GISS, and MPI) appear to generally capture the spatial pattern of the global SST warming mode, as represented by the leading mode of the REOF of the global SST anomalies. Several models (GFDL-ESM2M, HadGEM2-CC, MIROC5, and MRI) cannot capture this mode as the leading REOF mode. The realism of this mode appears to be correlated to, and perhaps influences, the relationship between the global SST warming mode and changes of rainfall over the SC US. Only CCSM4 appears to qualitatively capture the observed relationship between the increase of rainfall over the SC US and the global SST warming mode. This raises a question as to whether the multi-model ensemble projections could adequately represent the response of the regional rainfall, at least for SC US to global warming that is central to future climate projections.

Ensemble projections by the RCP4.5 and RCP8.5 experiments for the period of 2074-2100 are compared to those simulated by the historical simulations for the period of 1979-2005, to assess future changes over the SC US. To determine potential influences of models' quality on regional climate projection, we compare the multi-model ensemble projections with and without the under-performing or "U" models. Both multi-model ensemble projections consistently project that a) the occurrence of Tmax ranging from 28°C to 43°C or 82.4°F to 109.4°F will increase by 25% to 50% in the future for the RCP4.5 scenario relative its occurrence in the recent past , and its frequency of occurrence will increase 50%-100% for the RCP8.5 scenario. The occurrence of warm Tmin (25°C- 30°C or 77°F - 86°F) increases

strongly. The occurrence of below freezing Tmin (<0˚C) will decrease under the RCP4.5 scenario. Under the high emission RCP8.5 scenario, the occurrence of Tmin exceeding 25˚C (77 ˚C) will increase, whereas the occurrence of colder Tmax (<0˚C) will decrease. Under the RCP8.5 scenario, the increase in Tmin could be several times greater than observed increases in the recent past. Removal of the under-performing models from the multi-models ensemble projections does not change the projections. The non-rainy and light-rainy days increase and occurrence of medium rainrate decrease in future under both RCP scenarios. The distribution of PDF of the P-ET does not change significantly under the RCP4.5 scenario, whereas under the RCP8.5 scenario, the occurrence of weak negative P-ET increases and that of weak positive P-ET decreases and the forced change becomes more robust under this stronger forcing scenario.

There are large discrepancies in projected changes of the distribution of rainrate, P, ET and P-ET between individual models. The under-performing models tend to be outliers in projecting these changes. Nevertheless, the multi-model ensemble projection suggests an increase of P and ET in winter, spring and fall, and decrease of P and ET in summer. The strong increase of ET generally out-weighs weak increases of rainfall in winter, spring and fall, leading to increased net surface water deficits in these seasons, especially under the RCP8.5 scenario. The removal of the under-performing models from the multi-model ensemble projections leads to even stronger projected decreases of P-ET in these seasons.

One of the main limitations of our assessment is its insufficient representation of the statistical distributions of the climate variables we evaluated due to both short duration of available observations, model simulations and limited ensemble members of simulations. For the regions such as SC US, multi-model ensembles cannot effectively remove common biases among the majority of the models. However, a large number of ensemble simulations by the "best performing models" could provide an alternative and complementary approach to reduce the uncertainties of the climate projections.

References

Barlow, M., S. Nigam and E. H. Berbery 2001: ENSO, Pacific decadal variability and U. S. summertime precipitation, drought and streamflow. J. Climate 14,2105-2127.

Barnett, T. P., D. W. Pierce, and R. Schnur, 2001: Detection of Anthropogenic Climate Change in the World's Oceans, *Science*, **292**, 270-274.

Barnston, A. G., and R. E. Livezey, 1987: Classification, seasonality and persistence of low-frequency atmospheric circulation patterns, *Mon. Wea. Rev.*, **115**, 1083-1126.

Cook, K. H., E. K. Vizy, Z. S. Launer, and C. M. Patricola, 2008: Springtime Intensification of the Great Plains Low-Level Jet and Midwest Precipitation in GCM Simulations of the Twenty-First Century, *J. Climate*, **21**, 6321-6340.

Collins W. J., N. Bellouin, M. Doutriaux-Boucher, N. Gedney, P. Halloran, T. Hinton, J. Hughes, C. D. Jones, M. Joshi, S. Liddicoat, G. Martin, F. O'Connor, J. Rae, C. Senior, S. Sitch, I. Totterdell, A. Wiltshire, S. Woodward, 2011: Development and evaluation of an Earth-system model – HadGEM2, *Geosci Model Dev Discuss,* **4**(2),997-1062, doi:10.5194/gmdd-4-997-2011.

Dai, A., K. E. Trenberth, and T. T. Qian, 2004: A global dataset of Palmer Drought Severity Index for 1870-2002: Relationship with soil moisture and effects of surface warming, *J. Hydrometeor.*, **5**, 1117-1130.

Deser, C., A. Phillips, V. Bourdette, and H. Y. Teng, 2012: Uncertainty in climate change projections: the role of internal variability, *Clim. Dyn.*, **38**, 527-546.

Dunne, J. P., J. G. John, A. J. Adcroft, S. M. Griffies, R.W. Hallberg, E. Shevliakova, R. J. Stouffer, W. Cooke, K. A. Dunne, M. J. Harrison, J. P. Krasting, S. L. Malyshev, P. C. D. Milly, P. J. Phillipps, L. A. Sentman, B. L. Samuels, M. J. Spelman, M. Winton, A. T. Wittenberg, and N. Zadeh, 2012: GFDL's ESM2 global coupled climate-carbon Earth System Models Part I: Physical formulation and baseline simulation characteristics, *J. Climate*, **25**, 6646-6665, doi:10.1175/jcli-d-11-00560.

Enfield, D. and D. A. Mayer, 1997:,Tropical Atlantic sea surface temperature variability and its relation to El Nino-Southern Oscillation. J. Geophy. Res.102,929-845.

Fannin, B. 2012: Updated 2011 Texas agricultural drought losses total $7.62 billion. AgriLifeTODAY.

Fernando D. N., K. C. Mo, R. Fu, B. R. Scanlon, R. Solis, L. Yin, A. Bowerman, R. Mace and J. R. Mioduszewski, in-review: What caused the onset, intensification, and recovery of the 2011 drought over Texas?, *Proc. Natl. Acad. Sci. - Plus*, Submitted

Gent, P. R., G. Danabasoglu, L. J. Donner, M. M. Holland, E. C. Hunke, S. R. Jayne, D. M. Lawrence, R. B. Neale, P. J. Rasch, M. Vertenstein, P. H. Worley, Z.-L. Yang, and M. Zhang, 2011: The Community Climate System Model Version 4, *J. Climate*, **24**(19),4973-4991, doi:10.1175/2011jcli4083.

L. Goddard, S. J. M. S. E. Z. C. F. R. R. B. M. A. C. (2001), Current approaches to seasonal to interannual climate predictions, *International Journal of Climatology*, *21*, 1111-1152.

Gleckler, P. J., K. E. Taylor, and C. Doutriaux, 2008: Performance metrics for climate models, *J. Geophys. Res.*, **113**, D06104.

Grassi, B., G. Redaelli, P. O. Canziani, and G. Visconti, 2012: Effects of the PDO phase on the tropical belt width, *J. Climate*, **25**, 3282-3290.

Hibbard, K. A., G. A. Meehl, P. Cox, and P. Friedlingstein, 2007: A strategy for climate change stabilization experiments, *EOS*, **88**, 217, 219, 221.

Higgins, R. W., J.E. Janowiak, and Y.-P. Yao, 1996: A Gridded Hourly Precipitation Data Base for the United States (1963-1993), *NCEP/Climate Prediction Center ATLAS No. 1,* U. S. D. O. C., *National Oceanic and Atmospheric Administration, National Weather Service*, Ed.

Higgins, R. W., Y. Yao, X. L. Wang, 1997: Influence of the North American Monsoon System on the U.S. Summer Precipitation Regime. *J. Climate*, **10**, 2600-2622.

Hoerling, M. and co-authors 2013: Anatomy of an extreme event. J. Climate. In press.

Hong, S.-Y., and E. Kalnay, 2002: The 1998 Oklahoma–Texas Drought: Mechanistic Experiments with NCEP Global and Regional Models. *Journal of Climate*, **15,** 945-963.

Huang, J, H. van den Dool and K. P. Georgakakus 1996: Analysis of model calculated soil moisture over the United States (1931-1993) and applications to long range temperature forecasts. J. Climate 9, 1350-1362.

Hu, Q. and S. Feng, 2008: Variation of the North American Summer Monsoon Regimes and the Atlantic Multidecadal Oscillation, *J. Climate*, **21**(11), 2371-2383.

Jiang, X. Y. and Z. L. Yang, 2012: Projected changes of temperature and precipitation in Texas from downscaled global climate models, *Clim. Res.*, **53**, 229-244.

Kalnay, E., M. Kanamitsu, R. Kistler, W. Collins, D. Deaven, L. Gandin, M. Iredell, S. Saha, G. White, J. Woollen, Y. Zhu, M. Chelliah, W. Ebisuzaki, W. Higgins, J. Janowiak, K. Mo, C. Ropelewski, J. Wang, A. Leetma, R. Reynolds, R. Jenne, and D. Joseph, 1996: The NCEP-NCAR 40-Year Reanalysis Project, *Bull. Amer. Meteor. Soc.*, **77**, 437–471.

Karl, T. R., J. M. Melillo, T. C. Peterson, D. M. Anderson, D. F. Boesch, V. Burkett, L. M. Carter, S. J. Cohen, N. B. Grimm, J. L. Hatfield, K. Hayhoe, A. Janetos, J. A. Kaye, J. Lawrimore, J. McCarthy, A. D. McGuire, E. Miles, E. Mills, J. T. Overpeck, J. Patz, R. Pulwarthy, B. Santer, M. J. Savonis, H. G. Schwartz, E. Shea, J. Stone, B. H. Udall, J. Walsh, M. F. Wehner, T. J. Wilbanks, and D. Wuebbles, 2009: *Global Climate Change Impacts in the United States: A State of Knowledge Report from the U.S. Global Change Research Program,* New York, Cambridge University Press.

Kistler, R., E. Kalnay, W. Collins, S. Saha, G. White, J. Woollen, M. Chelliah, W. Ebisuzaki, M. Kanamitsu, V. Kousky, H. van den Dool, R. Jenne, and M. Fiorino, 2001: The NCEP-NCAr 50-Year reanalysis: Monthly means CD-ROM and documentation, *Bull. Amer. Met. Soc.,* **28**, 2, 247-267.

Koster, R. and Co authors 2004: Regions of strong coupling between soil moisture and precipitation. Science, 305, 1138-1140.

Kushnir, Y., R. Seager, M. F. Ting, N. Naik, and J. Nakamura, 2010: Mechanisms of Tropical Atlantic SST Influence on North American Precipitation Variability, *J. Climate*, **23**, 5610-5628.

Lyon, B., and R. M. Dole, 1995: A diagnostic comparison of the 1980 and 1988 U.S. summer heat wave–droughts. *J. Climate*, **8**, 1658–1675.

Li, W. H., L. F. Li, R. Fu, Y. Deng, and H. Wang, 2011: Changes to the North Atlantic Subtropical High and Its Role in the Intensification of Summer Rainfall Variability in the Southeastern United States, *J. Climate*, **24**, 1499-1506.

Madden, R. and J. Williams, 1978: The correlation between temperature and 1071 precipitation in the United States and Europe, *Mon. Wea. Rev.*, **106**, 142-147.

Martin, G. M., N. Bellouin, W. J. Collins, I. D. Culverwell, P. R. Halloran, S. C. Hardiman, T. J. Hinton, C. D. Jones, R. E. McDonald, A. J. McLaren, F. M. O'Connor, M. J. Roberts, J. M. Rodriguez, S. Woodward, M. J. Best, M. E. Brooks, A. R. Brown, N. Butchart, C. Dearden, S. H. Derbyshire, I. Dharssi, M. Doutriaux-Boucher, J. M. Edwards, P. D. Falloon, N. Gedney, L. J. Gray, H. T. Hewitt, M. Hobson, M. R. Huddleston, J. Hughes, S. Ineson, W. J. Ingram, P. M. James, T. C. Johns, C. E. Johnson, A. Jones, C. P. Jones, M. M. Joshi, A. B. Keen, S. Liddicoat, A. P. Lock, A. V. Maidens, J. C. Manners, S. F. Milton, J. G. L. Rae, J. K. Ridley, A. Sellar, C. A. Senior, I. J. Totterdell, A. Verhoef, P. L. Vidale, and A.Wiltshire, 2011: The HadGEM2 family of Met Office Unified Model climate configurations, *Geosci. Model Dev.,* **4**(3), 723-757, doi:10.5194/gmd-4-723-2011.

Maurer, E. P., A. W. Wood, J. C. Adam, D. P. Lettenmaier, and B. Nijssen, 2002: A long term hydrologically based dataset of land surface fluxes and states for the conterminous United States. *J. Climate*, **15**, 3237-3251.

McCabe, G. J., M. A. Palecki, and J. L. Betancourt, 2004: Pacific and Atlantic Ocean influences on multidecadal drought frequency in the United States, *Proc. Natl. Acad. Sci.*, **101**, 4136-4141.

McKee, T. B., N. J. Doesken, and J. Kleist, 1993: The relationship of drought frequency and duration to time scales.   Preprints, Eighth conf. on Applied Climatology. Anaheim Ca, AMS, 179-184.

McKee, T. B., N. J. Doesken, and J. Kleist, 1995: Drought monitoring with multiple time scales. Preprints, Ninth conf. on Applied Climatology. Dallas Tx, AMS, 233-236.

Meehl, G. A., C. Covey, T. L. Delworth, M. Latif, B. McAveney, J. F. B. Mitchell, R. J. Stouffer, and K. E. Taylor, 2007b: The WCRP CMIP3 multimodel dataset: A new era in climate change research, *Bull. Amer. Meteor. Soc.*, **88**, 1383-1394, doi:10.1175/BAMS-88-9-1383.

Mesinger, F. and coauthors 2006: North American regional reanalysis. Bull. Amer. Meteor. Soc. 87, 343-360.

Mishra, A. K. and V. P. Singh, 2009: Analysis of drought severity-area-frequency curves using a general circulation model and scenario uncertainty, *J. Geophy. Res.,* **114**, D06120, , doi:10.1029/2008JD010986.

Mo, K. C. , 2011: Drought onset and recovery over the United States . J. Geophy. Res. Doi: 10.1029:/2011JD016168.

Mo, K. C., J. E. Schemm, and S. H. Yoo : 2009: ENSO and the Atlantic multi decadal oscillation on drought over the United States. J. *Climate,* **22**, 5962-5982.

Mo, Kingtse C., J. R. Zimmerman, E. Kalnay, M. Kanamitsu, 1991: A GCM Study of the 1988 United States Drought. *Mon. Wea. Rev.*, **119**, 1512–1532.

Moss, R. H., J. A. Edmonds, K. A. Hibbard, M. R. Manning, S. K. Rose, D. P. van Vuuren, T. R. Carter, S. Emori, M. Kainuma, T. Kram, G. A. Meehl, J. F. B. Mitchell, N. Nakicenovic, K. Riahi, S. J. Smith, R. J. Stouffer, A. M. Thomson, J. P. Weyant and T. J. Wilbanks, 2010: The next generation of scenarios for climate change research and assessment, *Nature*, **463**, 747-756, doi:10.1038/nature08823.

Myoung, B. and J. W. Nielsen-Gammon: 2010. The Convective Instability Pathway to Warm Season Drought in Texas. Part I: The role of convective inhibition and its modulation by soil moisture. J. Climate, 23,4461-4488.

Mantua, N.J. and S.R. Hare, Y. Zhang, J.M. Wallace, and R.C. Francis 1997: <u>A Pacific interdecadal climate oscillation with impacts on salmon production</u>. Bulletin of the American Meteorological Society, 78, pp. 1069-1079.

Namias 1991, "Spring and summer drought over the contiguous U.S.--Causes and prediction." *J. Cimate*, **4**, 54-65.

Nigam, S., B. Guan, and A. Ruiz-Barradas, 2011: Key role of the Atlantic Multidecadal Oscillation in 20th century drought and wet periods over the Great Plains, *Geophys. Res. Lett.*, **38**, L16713, doi:10.1029/2011GL048650.

O'Lenic, E. A., and R. E. Livezey, 1988: Practical considerations in the use of Rotated Principal Component Analysis (RPCA) in diagnostic studies of upper-air height fields, *Mon. Wea. Rev.*, **116**, 1682-1689.

Palmer, T. N. (1993), Extended-Range Atmospheric Prediction and the Lorenz Model, *Bulletin of the American Meteorological Society*, *74*, 49-65.

Pierce, D. W., T. P. Barnett, B. D. Santer, and P. J. Gleckler, 2009: Selecting global climate models for regional climate change studies, *Proc. Natl. Acad. Sci.*, **106**(21), 8441-8446.

Raddatz, T., C.Reick, W. Knorr, J. Kattge, E. Roeckner, R. Schnur, K. G. Schnitzler, P. Wetzel, and J. Jungclaus, 2007: Will the tropical land biosphere dominate the climate–carbon cycle feedback during the twenty-first century? *Clim. Dyn.* **29**(6),565-574, doi:10.1007/s00382-007-0247-8.

Richman, M. B., 1987: Rotation of principal components: A reply, *J. Climatology*, **7**, 511-520.

Rodell, M., P. R. Houser, U. Jambor, J. Gottschalck, K. Mitchell, C-J. Meng, K. Arsenault, B. Cosgrove, J. Radakovich, M. Bosilovich, J. K. Entin, J. P. Walker, D. Lohmann, and D. Toll, 2004: The global land data assimilation system, *Bull. Amer. Meteor. Soc.*, **85**, 381-393.

Ropelewski, C. F., and M. S. Halpert (1986), North American precipitation and temperature patterns associated with the El Nino/Southern Oscillation. *Mon. Wea. Rev.*, **114**, 2352-2362

------------, and ---------- (1989), Precipitation patterns associated with the high index   phase of the Southern Oscillation. *J. Climate,* **2**, 268-284.

Schubert S. D., and coauthors (2009), A USCLIVAR project to assess and compare the responses of global climate models to drought related SST forcing patterns: Overview and Results. *J. Climate* **22**, 5251-5272.

Schmidt, G. A., R. Ruedy, J. E. Hansen, I. Aleinov, N. Bell, M. Bauer, S. Bauer, B. Cairns, V. Canuto, Y. Cheng, A. Del Genio, G. Faluvegi, A. D. Friend , T. M. Hall, Y. Hu, M. Kelley, N. Y. Kiang , D. Koch, A. A. Lacis , J. Lerner, K. K. Lo, R. L. Miller, L. Nazarenko, V. Oinas, J. Perlwitz, D. Rind, A. Romanou, G. L. Russell, M. Sato, D. T. Shindell, P. H. Stone, S. Sun, N. Tausnev, D. Thresher, and M. S. Yao, 2006: Present-Day Atmospheric Simulations Using GISS ModelE: Comparison to In Situ, Satellite, and Reanalysis Data, *J. Climate,* **19**, 153-192, doi:10.1175/jcli3612.1.

Seager, R., M. F. Ting, I. Held, Y. Kushnir, J. Lu, G Vecchi, H. P. Huang, N. Harnik, A. Leetmaa, N. C. Lau, C. H. Li, J. Velez, N. Naik, 2007: Model Projections of an Imminent Transition to a More Arid Climate in Southwestern North America, *Science*, **316**, 1181-1184, doi: 10.1126/science.1139601.

Shukla, J., and Kinter III, J.L. (2006), Predictability of seasonal climate variations: a pedagogical review, in *Predictability of Weather and Climate*, edited by T. Palmer, and Hagedorn, R., pp. 306-341, Cambridge University Press.

Smith, T. M., R. W. Reynolds, R. E. Livezey, and D. C. Stokes (1996), Reconstruction of historical sea surface temperatures using empirical orthogonal functions. *J. Climate*, **9,** 1403-1420.

Stevenson, S. L., 2012: Changes to ENSO strength and impacts in the CMIP5 models, *J. Geophys. Res.*, In press.

Stillwell, A. S., C. W. King, M. E. Webber, I. J. Duncan, and A. Hardberger. 2010: The energy-water nexus in Texas.*Ecology and Society* **16**(1): 2. [online] URL: http://www.ecologyandsociety.org/vol16/iss1/art2/

Taylor, K. E., R. J.Stouffer, and G. A.Meehl, 2012: An Overview of CMIP5 and the Experiment Design, *Bull. Amer. Met. Soc.,* **93**(4), 485-498, doi:10.1175/bams-d-11-00094.

Ting, M. and H. Wang 1997: Summertime U. S. precipitation variability and its relation to Pacific sea surface temperature. J. Climate,10,1853-1873.

Trenberth, K. E., G. W. Branstator, and P. A. Arkin, 1988: Origins of the 1988 North American drought. *Science,* **242**, 1640–1645.

Trenberth, K. E., P.D. Jones, P. Ambenje, R. Bojariu, D. Easterling, A. Klein Tank, D. Parker, F. Rahimzadeh, J.A. Renwick, M. Rusticucci, B. Soden, and P. Zhai, 2007: Observations: Surface and Atmospheric Climate Change. In: Climate Change 2007: The Physical Science Basis, *Contribution of Working Group I to the Fourth Assessment Report of the Intergovernmental Panel on Climate Change* [Solomon, S., D. Qin, M. Manning, Z. Chen, M. Marquis, K.B. Averyt, M. Tignor and H.L. Miller (eds.)].

Vose, R. S, T. C. Peterson, R. L. Schmoyer, J. K. Eischeid, P. M. Steurer, R. R. Heim, and T. R. Karl, 1993: The GlobalHistorical Climatology Network: Long-term monthly temperature, precipitation, and pressure data, *Fourth AMS Symposium on Global Change Studies,* Anaheim, CA., January 17-22 1993.

Watanabe, M., T. Suzuki, R. O'ishi, Y. Komuro, S. Watanabe, S. Emori, T. Takemura, M. Chikira, T.

Ogura, M. Sekiguchi, K. Takata, D. Yamazaki, T. Yokohata, T. Nozawa, H. Hasumi, H. Tatebe, and M. Kimoto, 2010: Improved Climate Simulation by MIROC5: Mean States, Variability, and Climate Sensitivity, *J. Climate*, **23**, 6312–6335, doi: http://dx.doi.org/10.1175/2010JCLI3679.1.

Wang, H., R. Fu, A. Kumar, and W. H. Li, 2010: Intensification of Summer Rainfall Variability in the Southeastern United States during Recent Decades, *J. Hydrometeor.*, **11**, 1007-1018.

Wang, H., S.D. Schubert, M. J. Suarez, J. Chen, M. Hoerling, A. Kumar, and P. Pegion, 2009: Attribution of the seasonality and regionality in climate trends over the United States during 1950-2000", *J. Climate*, **22**, 2571-2590.

Wittengberg, A. T., 2009: Are historical records sufficient to constrain ENSO simulations?, *Geophys. Res. Lett.*, **36**, L12702, doi:10.1029/2009GL038710.

Xia, Y., Mike Ek, Heilin Wei and Jesse Ming 2011: Comparative analysis of relationships between NLDAS-2 forcing and model outputs. Hydrological. Processes doi:10.1002/hyp.8240.

Xie, P. P., M. Chen, and W, Shi (2010), CPC unified gauge based analysis of global daily precipitation. AMS 24th Conf. on hydrology. Jan 18-21, 2010, Atlanta, GA.

Yukimoto, S., H. Yoshimura, M. Hosaka, T. Sakami, H. Tsujino, M. Hirabara, T. Y. Tanaka, M. Deushi, A. Obata, H. Nakano, Y. Adachi, E. Shindo, S. Yabu, T. Ose, and A. Kitoh, 2011: Meteorological Research Institute Earth System Model Version 1 (MRI ESM1) - Model Description , *Technical Report of the Meteorological Research Institute,* **64**, 83pp (available from http://www.mri-jma.go.jp/Publish/Technical/index_en.html).

Annexure 1: Drought years and seasonal rainfall anomalies

(a) Standardized anomalies of MAM (beige) and JJA (orange) rainfall plotted against August values (current year) of the Palmer Drought Severity Index (PDSI) and the September (previous year) values of the 12-monthly Standardized Precipitation Index (SPI)
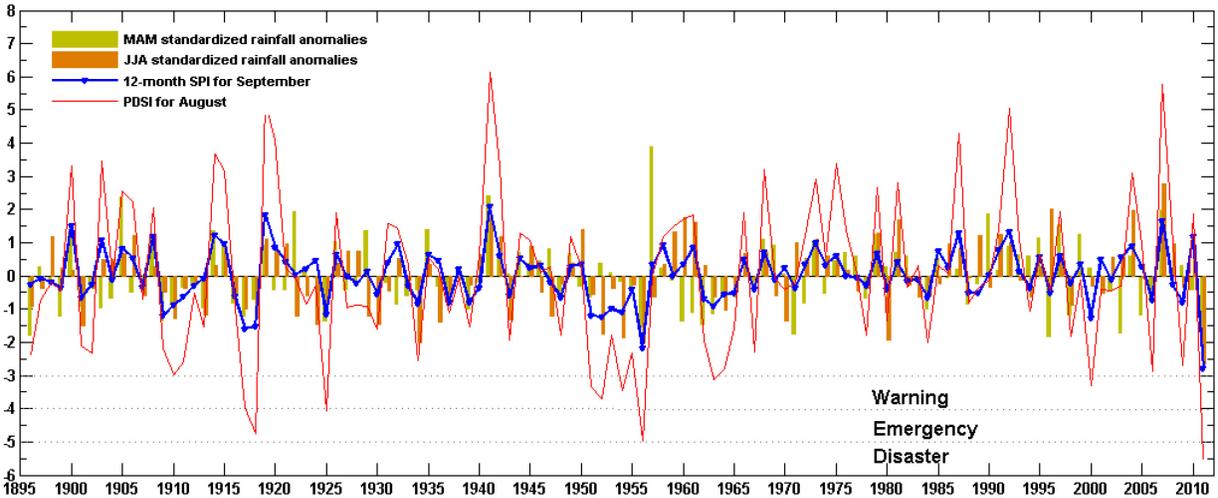
(b) Seasonal rainfall states and drought events since 1895

Season state	Events	Severe-to-extreme drought	Moderate drought
$DJF_{(dry)} \| MAM_{(dry)} \| JJA_{(dry)}$	23	12	6
$DJF_{(wet)} \| MAM_{(dry)} \| JJA_{(dry)}$	14	1	2
$DJF_{(dry)} \| MAM_{(dry)} \| JJA_{(wet)}$	15	2	0
$DJF_{(wet)} \| MAM_{(dry)} \| JJA_{(wet)}$	11	0	0
$DJF_{(dry)} \| MAM_{(wet)} \| JJA_{(dry)}$	16	3	2
$DJF_{(wet)} \| MAM_{(wet)} \| JJA_{(dry)}$	8	0	0
$DJF_{(dry)} \| MAM_{(wet)} \| JJA_{(wet)}$	9	0	0
$DJF_{(wet)} \| MAM_{(wet)} \| JJA_{(wet)}$	20	0	0
Total (years)	116	18	10

Seasonal state transitions for consecutive DJF, MAM and JJA seasons. Column 2 gives the number of years when each transition state prevailed. Columns 3 and 4 list the number of years when severe-to-extreme droughts, and moderate droughts, were associated with a particular transition state.

(c) Severe-to-extreme drought years by rainfall state and La Niña (LN) state (depicted for years post 1950)

DJF$_{(dry)}$|MAM$_{(dry)}$|JJA$_{(dry)}$: 1902, 1911, 1917, 1918, 1925, 1951 (LN), 1954(LN), 1955(LN), 1956(LN), 1963, 2006(LN),2011(LN)

DJF$_{(dry)}$|MAM$_{(wet)}$|JJA$_{(dry)}$: 1998

DJF$_{(dry)}$|MAM$_{(dry)}$|JJA$_{(wet)}$: 1971(LN), 1996(LN)

DJF$_{(dry)}$|MAM$_{(wet)}$|JJA$_{(dry)}$: 1952, 1953, 2000(LN)

Year(s) when La Niña induced winter drought that ended in spring: 2000 (hence 1/9 = 11%)